

Semi-Blind Cascaded Channel Estimation for Reconfigurable Intelligent Surface Aided Massive MIMO

Zhen-Qing He, Hang Liu, Xiaojun Yuan, Ying-Jun Angela Zhang, and Ying-Chang Liang

Abstract—Reconfigurable intelligent surface (RIS) is envisioned to be a promising green technology to reduce the energy consumption and improve the coverage and spectral efficiency of multiple-input multiple-output (MIMO) wireless networks. In a RIS-aided MIMO system, the acquisition of channel state information (CSI) is important for achieving passive beamforming gains of the RIS, but is also challenging due to the cascaded property of the transmitter-RIS-receiver channel and the lack of signal processing capability of the large number of passive RIS elements. The state-of-the-art approach for CSI acquisition in such a system is a pure training-based strategy that hinges on a long sequence of pilot symbols. In this paper, we investigate semi-blind cascaded channel estimation for RIS-aided massive MIMO systems, in which the receiver jointly estimates the channels and the partially unknown transmit signals with a small number of pilot sequences. Specifically, we formulate the semi-blind channel estimation as a trilinear matrix factorization task. Under the Bayesian inference framework, we develop a computationally efficient iterative algorithm using the sum-product approximate message passing principle to resolve the trilinear inference problem. Meanwhile, we present an analytical framework to characterize the theoretical performance bound of the proposed algorithm in the large-system limit. Extensive simulation results demonstrate the effectiveness of the proposed semi-blind channel estimation algorithm.

Index Terms—Cascaded channel estimation, massive MIMO, approximate message passing, reconfigurable intelligent surface, replica method.

I. INTRODUCTION

A. Motivation

MASSIVE multiple-input multiple-output (MIMO) technology, a key component of the fifth-generation (5G) wireless communications systems, has received considerable research interests in both academia and industry in recent years [1]–[3]. Although massive MIMO has huge potentials to improve the spectral efficiency and boost the system throughput, the wireless propagation links between the transmitter and the receiver might suffer from deep fading and shadowing due to unfavorable propagation conditions such as in urban areas or indoor environments. More recently, reconfigurable intelligent surface (RIS) [4]–[6], also known as intelligent reflecting surface [7], has emerged as a promising technology to improve the

link reliability of MIMO wireless networks as it can artificially reconfigure the wireless propagation environment. In contrast to a conventional amplify-and-forward relay, a RIS consists of a large number of low-cost and passive elements without radio frequency chains and additional thermal noise. Owing to the advances of programmable metamaterials [8], it has become feasible to reconfigure the phase shifts of RISs in real time. As such, the RIS-aided massive MIMO has been envisioned as a key enabler for the next generation wireless communications systems to enhance network coverage and achieve smart radio environments [6], [9]–[11].

Specifically, the passive beamforming gain of RIS-aided MIMO systems can be achieved by adjusting the phase shifts of the RIS elements so that the desired signals can be added constructively at the receiver. Extensive recent researches have verified the capacity advantage of RIS-aided MIMO systems by passive beamforming design under various criteria [4], [7], [12], [13]. However, to realize the full advantage of RISs, the availability of the channel state information (CSI) plays a critical role. As a nearly-passive device, RISs are generally not equipped with any radio frequency chains and are not capable of performing any baseband processing functionality. Consequently, the transmitter-RIS and RIS-receiver channels cannot be estimated via traditional MIMO channel estimation methods. Currently, the design of the CSI acquisition method in RIS-aided MIMO systems is still in its infancy and the state-of-art approaches (see e.g., [14]–[22]) are pure training-based schemes that require prohibitively long training pilots. This motivates us to explore new channel estimation techniques that reliably estimate the RIS channels with a reduced number of pilot overhead.

B. Contributions

In this paper, we investigate semi-blind cascaded channel estimation for the RIS-aided uplink massive MIMO system, where a multi-antenna base station (BS) communicates with multiple single-antenna users with the help of a RIS. In particular, the receiver can simultaneously estimate the channel coefficients and detect the transmitted data of users using a small number of pilots. We aim to design a computationally efficient semi-blind channel estimation algorithm and characterize its asymptotic performance in the large-system limit. The main contributions of our work are summarized as follows.

- 1) We formulate the semi-blind cascaded channel estimation problem in the RIS-aided MIMO system as a trilinear estimation problem, where the received signal consists of

Z.-Q. He, X. Yuan, Y.-C. Liang are with the National Key Laboratory of Science and Technology on Communications and also with the Center for Intelligent Networking and Communications, University of Electronic Science and Technology of China, Chengdu 611731, China (e-mail: {zhenqinghe; xjyuan; ycliang}@uestc.edu.cn).

H. Liu and Y.-J. A. Zhang are with the Department of Information Engineering, The Chinese University of Hong Kong, Shatin, New Territories, Hong Kong SAR (e-mail: {lh117; yjzhang}@ie.cuhk.edu.hk).

the product of the RIS-BS channel matrix, the user-RIS channel matrix, and the transmit data matrix. Additionally, unlike the existing training-based works [14]–[22] that estimate the channel coefficients and the transmitted signal separately, we consider a joint estimation of the both channels and the payload data with a small number of pilots.

- 2) We develop a computationally efficient iterative algorithm to approximately solve the trilinear estimation problem based on the Bayesian minimum mean square error (MMSE) criterion. Specifically, we adopt the approximate message passing (AMP) framework [23]–[25] to approximately calculate the marginal posterior distributions of the channel coefficients and the unknown transmit data. The proposed algorithm has low per-iteration complexity, since it only needs to update the means and variances of the messages and involves basic matrix multiplication.
- 3) Based on the replica method from statistical physics [26], [27], we analyse the asymptotic minimum mean square errors (MSEs) of the posterior mean estimators in the large-system limit. We show that with perfect knowledge of prior distributions of the channels and data, the MSEs of the posterior mean estimators can be determined by the fixed point of a set of scalar equations. Extensive numerical experiments under Rayleigh fading channels and quadrature phase-shift keying (QPSK) signal show that the proposed algorithm can well approach the asymptotic MSE bound, demonstrating the efficiency of the proposed message passing algorithm.

C. Related Work

The cascaded channel estimation problem for RIS-aided MIMO systems has been investigated in a variety of recent works using different approaches. For example, in [14] and [15], the on-off reflection pattern was utilized for the RIS channel estimation. Unlike [14] using the linear minimum mean square error criterion, [15] developed a two-stage channel estimation algorithm that includes a sparse matrix factorization stage and a matrix completion stage. By appropriately designing the RIS reflection coefficients, [16] proposed a three-phase channel estimation scheme based on the correlation among user-RIS-BS reflection channels of different users, whereas [19] proposed a channel estimation scheme based on minimizing the Cramér-Rao lower bound. By leveraging the sparsity of RIS channels, [17] developed a compressed sensing based scheme to estimate the user-RIS-BS cascaded channel. In [18], the authors formulated the RIS channel estimation problem as a matrix-calibration based matrix factorization problem. In [20], the authors proposed a channel estimation framework based on the PAEAllel Factor (PARAFAC) decomposition. Besides these, machine learning based RIS channel estimation methods were also introduced. For instance, in [21] a twin convolutional neural network architecture was designed to estimate the RIS channels and in [22] a deep denoising neural network was used to assist the estimation of the compressive RIS channels. In addition, [28] considered the channel estimation of wideband RIS-aided orthogonal frequency division multiplexing system.

The above mentioned works all belong to the training-based approach that needs a long duration of pilot sequences. In the training-based approach, each transmission frame is divided into two phases: a training phase and a data transmission phase. In the training phase, pilots are transmitted to facilitate the channel estimation at the receiver side. In the data transmission phase, unknown data are transmitted and the receiver performs detection based on the estimated channel in the training phase. Compared with the two separate phases for channel estimation and data detection, semi-blind channel estimation approach is able to improve the channel estimation performance because the estimated data can be utilized as soft pilots to enhance the channel estimation accuracy. This approach has proven successful in conventional massive MIMO semi-blind channel estimation [29]–[31]. Note that the semi-blind channel estimation problem in conventional massive MIMO systems is a special case of our work when the user-RIS-BS link is absent.

As a final remark, we note that the on-off phase shift design in this work is similar to that in our prior work [15]. However, this work significantly improves upon our prior work [15] in the following aspects. First, the direct and indirect link channels are estimated separately in [15], whereas we consider the joint estimation of both the direct and indirect link channels. Second, the work in [15] considers only the training-based channel estimation with all transmit data being as pilots by two separate stages: sparse matrix factorization and matrix completion. Instead, the current work treats only small partial transmit data being as pilots and simultaneously performs channel estimation and signal detection under the Bayesian MMSE criterion. The associated problem hence becomes a trilinear inference problem that is far more complicated than the bilinear inference problem in [15]. Third, the asymptotic MMSE performance is analyzed in our work. Simulation results show that compared with the method in [15], the proposed algorithm has a significant performance improvement even with a much smaller number of pilots and is able to perform close to the asymptotic MMSE bound in various parameter settings.

D. Organization and Notation

The remaining sections are organized as follows. Sections II and III introduce the system model and the problem formulation, respectively. Section IV presents the semi-blind channel estimation algorithm, analyses the computational complexity, and discusses the technical details. Section IV-D elaborates the asymptotic performance bound by the replica method. Section VI evaluates the performance of the proposed algorithm via extensive numerical experiments. Finally, Section VII concludes the paper.

Notation: We use $\mathbb{C}^{m \times n}$ to represent the space of $m \times n$ dimensional complex number. The superscripts “*”, “T”, and “H” denote the conjugate, the transpose, and the conjugate transpose, respectively. For a vector $\mathbf{x} \in \mathbb{C}^n$, we use x_i to represent its i -th element. For a matrix $\mathbf{X} \in \mathbb{C}^{m \times n}$, we use x_{ij} , $\mathbf{x}_i^T \in \mathbb{C}^n$, $\mathbf{x}_j \in \mathbb{C}^m$, and $\text{tr}(\mathbf{X})$ to denote its (i, j) -entry, its i -th row, its j -th column, and its trace when $m = n$, respectively. For $x \in \mathbb{C}$, $|x|$ and $\angle x$ denote its amplitude and phase, respectively. The $\|\cdot\|_2$ and $\|\cdot\|_F$ stand for the ℓ_2 -norm of

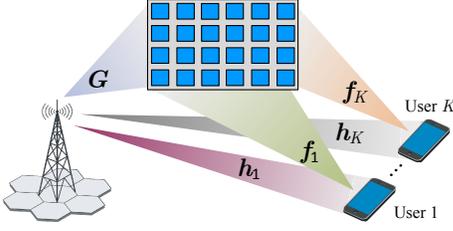


Fig. 1. A RIS-aided massive MIMO system.

a vector and the Frobenius norm of a matrix, respectively. We use $\mathbf{x} \sim \mathcal{N}(\mathbf{x}, \boldsymbol{\mu}; \boldsymbol{\Sigma})$ and $\mathbf{x} \sim \mathcal{CN}(\mathbf{x}, \boldsymbol{\mu}; \boldsymbol{\Sigma})$ denote that \mathbf{x} follows the real normal and complex circularly-symmetric normal distributions with mean $\boldsymbol{\mu}$ and covariance $\boldsymbol{\Sigma}$, respectively. In addition, we use \propto , $\delta(\cdot)$, $j \triangleq \sqrt{-1}$, $\mathbf{0}$, \mathbf{I}_m , $\text{Re}(\cdot)$, \odot , $\mathbb{E}\{\cdot\}$, and $\text{var}\{\cdot\}$ to represent the equality up to a constant multiplicative factor, the Dirac delta function, the imaginary unit, the all-zero vector/matrix with a proper size, the $m \times m$ identity matrix, the real operator, the element-wise multiplication, the expectation operator, and the variance operator, respectively.

II. SYSTEM MODEL

We consider a RIS-aided uplink massive MIMO wireless system, as shown in Fig. 1, where the RIS consists of N passive reflect elements and the BS with M receive antennas serves K single-antenna users. The RIS is deployed to enhance the communication quality between the users and the BS. We assume quasi-static block-fading channels with coherence time T , i.e., the channels remain approximately constant within each transmission block of length T . The baseband equivalent channels from the RIS to the BS, from the users to the RIS, and from the users to the BS are denoted by $\mathbf{G} \in \mathbb{C}^{M \times N}$, $\mathbf{H} \triangleq [\mathbf{h}_1, \dots, \mathbf{h}_K] \in \mathbb{C}^{M \times K}$, and $\mathbf{F} \triangleq [\mathbf{f}_1, \dots, \mathbf{f}_K] \in \mathbb{C}^{N \times K}$, respectively, where \mathbf{h}_k and \mathbf{f}_k denote the channel vectors from the k -th user to the RIS and to the BS, respectively. Under perfect carrier and timing recovery, we can model the discrete-time received signal at the BS as

$$\mathbf{y}^{(t)} = \mathbf{G}(\mathbf{s}^{(t)} \odot (\mathbf{F}\mathbf{x}^{(t)})) + \mathbf{H}\mathbf{x}^{(t)} + \mathbf{w}^{(t)}, t = 1, \dots, T, \quad (1)$$

where $\mathbf{x}^{(t)}$ and $\mathbf{w}^{(t)}$ are the transmit symbols and the additive noise following from $\mathcal{CN}(0, \sigma^2 \mathbf{I}_M)$ at time instant t , respectively. In addition, $\mathbf{s}^{(t)} \triangleq [s_1^{(t)} | e^{j\angle s_1^{(t)}}, \dots, s_N^{(t)} | e^{j\angle s_N^{(t)}}]^\top$ is the reflect vector of the RIS with $\angle s_n^{(t)} \in (0, 2\pi]$ and $|s_n^{(t)}| \in \{0, 1\}$ being the phase shift and the on/off-state of the n -th RIS reflect element at time instant t , respectively. By summarizing all the T samples in (1), the received signal at the BS is compactly expressed as

$$\mathbf{Y} = \mathbf{G}(\mathbf{S} \odot (\mathbf{F}\mathbf{X})) + \mathbf{H}\mathbf{X} + \mathbf{W}, \quad (2)$$

where $\mathbf{Y} \triangleq [\mathbf{y}^{(1)}, \dots, \mathbf{y}^{(T)}] \in \mathbb{C}^{M \times T}$, $\mathbf{S} \triangleq [\mathbf{s}^{(1)}, \dots, \mathbf{s}^{(T)}] \in \mathbb{C}^{N \times T}$, $\mathbf{X} \triangleq [\mathbf{x}^{(1)}, \dots, \mathbf{x}^{(T)}] \in \mathbb{C}^{K \times T}$, and $\mathbf{W} \triangleq [\mathbf{w}^{(1)}, \dots, \mathbf{w}^{(T)}] \in \mathbb{C}^{M \times T}$. With the help of a programmable smart controller, the RIS is capable of dynamically rescattering the electromagnetic waves towards a desired user by adjusting $\{\mathbf{s}^{(t)}\}$. The design of $\{\mathbf{s}^{(t)}\}$ is usually referred to as passive beamforming [4], [7], [12].

Note that accurate information of \mathbf{G} , \mathbf{F} , and \mathbf{H} is essential

to the passive beamforming design. To acquire the CSI, a two-stage approach in [15] utilizes the on-off reflection pattern of the RIS to get a sparsity structure of $\mathbf{F}\mathbf{X}$. In this paper, by following [15], we set the phases of the on-state RIS elements to be zero and assume that \mathbf{S} consists of independent and identically distributed (i.i.d.) random variables drawn from the Bernoulli distribution with Bernoulli parameter ρ .¹ Herein, ρ is also called the sparsity level of \mathbf{S} to indicate the probability of turning on a RIS element (i.e., the sampling rate of the RIS). The 0-1 pattern of \mathbf{S} has also been exploited for passive information transfer [12] and modulating information bits [32]. Furthermore, we assume that \mathbf{G} , \mathbf{F} , \mathbf{H} , and \mathbf{X} are composed of i.i.d. variables with zero means and have the following separable probability density functions (PDFs):

$$p(\mathbf{G}) = \prod_{m=1}^M \prod_{n=1}^N p(g_{mn}), \quad p(\mathbf{F}) = \prod_{n=1}^N \prod_{k=1}^K p(f_{nk}), \quad (3)$$

$$p(\mathbf{H}) = \prod_{m=1}^M \prod_{k=1}^K p(h_{mk}), \quad p(\mathbf{X}) = \prod_{k=1}^K \prod_{t=1}^T p(x_{kt}). \quad (4)$$

This paper is concerned with the estimation of \mathbf{G} , \mathbf{F} , and \mathbf{H} with only a portion of the columns of \mathbf{X} being used as the pilots under the Bayesian inference framework, as will be addressed in the following sections.

III. PROBLEM FORMULATION

A. Semi-Blind Scheme

Suppose that for every T symbol duration, the first T_p symbol durations are utilized to transmit pilot sequences. The remaining $T_d = T - T_p$ time is used for data transmission. This is equivalent to partitioning \mathbf{X} as

$$\mathbf{X} = [\mathbf{X}_p, \mathbf{X}_d], \quad (5)$$

where $\mathbf{X}_p \in \mathbb{C}^{K \times T_p}$ and $\mathbf{X}_d \in \mathbb{C}^{K \times T_d}$ represent the pilot sequences and the unknown transmitted data, respectively. As a result, the PDF of \mathbf{X} can be expressed as

$$p(\mathbf{X}) = \underbrace{\left(\prod_{k=1}^K \prod_{t=1}^{T_p} p(x_{p,kt}) \right)}_{\triangleq p(\mathbf{X}_p)} \underbrace{\left(\prod_{k=1}^K \prod_{t=1}^{T_d} p(x_{d,kt}) \right)}_{\triangleq p(\mathbf{X}_d)}. \quad (6)$$

In particular, given a *known* pilot matrix $\overline{\mathbf{X}}_p$, we have

$$p(\mathbf{X}_p) = \delta(\mathbf{X}_p - \overline{\mathbf{X}}_p) = \prod_{k=1}^K \prod_{t=1}^{T_p} \delta(x_{p,kt} - \overline{x}_{p,kt}). \quad (7)$$

This work is to simultaneously estimate \mathbf{G} , \mathbf{F} , \mathbf{H} , and \mathbf{X}_d with given \mathbf{S} and $\mathbf{X}_p = \overline{\mathbf{X}}_p$. The usage of the partially known pilots $\mathbf{X}_p = \overline{\mathbf{X}}_p$ for implementing joint channel estimation and data detection is called semi-blind channel estimation. Note that the semi-blind channel estimation scheme in conventional massive MIMO systems [29]–[31] is a special case of the problem considered here when the user-RIS-BS link does not exist (i.e., $\mathbf{G} = \mathbf{F} = \mathbf{0}$).

¹We emphasize that the 0-1 matrix \mathbf{S} is deterministic to the receiver. That is, \mathbf{S} can be generated as a 0-1 pseudo-random matrix, and is known to both the RIS and the receiver by sharing a common random seed.

A close observation of (2) reveals that our semi-blind channel estimation problem belongs to the family of trilinear estimation problem, because (2) involves the multiplication of the three unknown matrices \mathbf{G} , \mathbf{F} , and \mathbf{X}_d . When the RIS is removed or turned off, i.e., $\mathbf{G} = \mathbf{F} = \mathbf{0}$, the semi-blind channel estimation problem is reduced to a bilinear estimation problem as only the two unknown terms \mathbf{H} and \mathbf{X}_d are mixed with each other.

Before proceeding, we would like to emphasize that scaling ambiguity exists between \mathbf{G} and \mathbf{F} for all estimation schemes. To see this, for any invertible diagonal matrix $\Phi \in \mathbb{C}^{N \times N}$, it holds that

$$\mathbf{G}(\mathbf{S} \odot (\mathbf{F}\mathbf{X})) = \mathbf{G}'(\mathbf{S} \odot (\mathbf{F}'\mathbf{X})), \quad (8)$$

where $\mathbf{G}' \triangleq \mathbf{G}\Phi$ and $\mathbf{F}' \triangleq \Phi^{-1}\mathbf{F}$. Nevertheless, it is sufficient to estimate the alternative \mathbf{G}' and \mathbf{F}' . This is because \mathbf{G}' and \mathbf{F}' can be regarded as effective channels in the sense that they have no impact on the passive beamforming design [15].

B. Bayesian MMSE Estimation

Using the mean square error metric, the MMSE estimators of \mathbf{G} , \mathbf{F} , \mathbf{H} , and \mathbf{X}_d solve for

$$\min_{\mathbf{G}} \mathbb{E} \left\{ \|\mathbf{G} - \tilde{\mathbf{G}}\|_{\mathbf{F}}^2 \right\}, \min_{\mathbf{F}} \mathbb{E} \left\{ \|\mathbf{F} - \tilde{\mathbf{F}}\|_{\mathbf{F}}^2 \right\}, \quad (9)$$

$$\min_{\mathbf{H}} \mathbb{E} \left\{ \|\mathbf{H} - \tilde{\mathbf{H}}\|_{\mathbf{F}}^2 \right\}, \min_{\mathbf{X}_d} \mathbb{E} \left\{ \|\mathbf{X}_d - \tilde{\mathbf{X}}_d\|_{\mathbf{F}}^2 \right\}, \quad (10)$$

where the expectations are evaluated over the joint distribution $p(\mathbf{Y}, \mathbf{G}, \mathbf{F}, \mathbf{H}, \mathbf{X}_d)$. According to Bayes' rule and the first-order optimal condition, the closed-form solutions of (9) and (10) are given by the following posterior mean estimators (also known as the MMSE estimators):

$$\hat{g}_{mn} = \mathbb{E}\{g_{mn}|\mathbf{Y}\}, \hat{f}_{nk} = \mathbb{E}\{f_{nk}|\mathbf{Y}\}, \quad (11a)$$

$$\hat{h}_{mk} = \mathbb{E}\{h_{mk}|\mathbf{Y}\}, \hat{x}_{d,kt} = \mathbb{E}\{x_{d,kt}|\mathbf{Y}\}, \quad (11b)$$

where the expectations are taken with respect to the marginal posterior distributions $p(g_{mn}|\mathbf{Y})$, $p(f_{nk}|\mathbf{Y})$, $p(h_{mk}|\mathbf{Y})$, and $p(x_{d,kt}|\mathbf{Y})$, respectively. The averaged MSEs of $\hat{\mathbf{G}}$, $\hat{\mathbf{F}}$, $\hat{\mathbf{H}}$, $\hat{\mathbf{X}}_d$ are defined as

$$\text{MSE}_{\mathbf{G}} \triangleq \frac{1}{MN} \mathbb{E} \left\{ \|\mathbf{G} - \hat{\mathbf{G}}\|_{\mathbf{F}}^2 \right\}, \quad (12a)$$

$$\text{MSE}_{\mathbf{F}} \triangleq \frac{1}{NK} \mathbb{E} \left\{ \|\mathbf{F} - \hat{\mathbf{F}}\|_{\mathbf{F}}^2 \right\}, \quad (12b)$$

$$\text{MSE}_{\mathbf{H}} \triangleq \frac{1}{MK} \mathbb{E} \left\{ \|\mathbf{H} - \hat{\mathbf{H}}\|_{\mathbf{F}}^2 \right\}, \quad (12c)$$

$$\text{MSE}_{\mathbf{X}_d} \triangleq \frac{1}{KT_d} \mathbb{E} \left\{ \|\mathbf{X}_d - \hat{\mathbf{X}}_d\|_{\mathbf{F}}^2 \right\}, \quad (12d)$$

respectively, where the expectations are over the joint posterior distribution $p(\mathbf{Y}, \mathbf{G}, \mathbf{F}, \mathbf{H}, \mathbf{X}_d)$.

Exact evaluation of the MMSE estimators in (11) are generally intractable because they involve high-dimensional integrations in the marginalization of the joint posterior distribution $p(\mathbf{G}, \mathbf{F}, \mathbf{H}, \mathbf{X}_d|\mathbf{Y})$. In the subsequent section, we develop a computationally efficient iterative algorithm to approximately calculate the MMSE estimators (11) based on the AMP framework [23]–[25]. We will then analyse the asymptotic performance of the theoretical MSEs in (12) to evaluate the performance of the proposed algorithm.

IV. SEMI-BLIND CHANNEL ESTIMATION VIA TRILINEAR APPROXIMATE MESSAGE PASSING

A. Factor Graph Representation

We begin with a factor graph representation of the posterior distribution of the unknown variables. By defining

$$\mathbf{C} \triangleq \mathbf{S} \odot (\mathbf{F}\mathbf{X}), \mathbf{Z} \triangleq \mathbf{G}\mathbf{C} + \mathbf{H}\mathbf{X}, \quad (13)$$

and using Bayes' theorem, the joint posterior distribution of \mathbf{G} , \mathbf{F} , \mathbf{H} , \mathbf{X} , \mathbf{Z} , and \mathbf{C} can be expressed by using the factorized distribution in (14) (shown at the bottom of the next page) where $p(\mathbf{Y}) = \int_{\mathbf{G}, \mathbf{F}, \mathbf{H}, \mathbf{X}, \mathbf{Z}, \mathbf{C}} p(\mathbf{Y}, \mathbf{G}, \mathbf{F}, \mathbf{H}, \mathbf{X}, \mathbf{Z}, \mathbf{C})$ is the normalization constant and

$$p(y_{mt}|\cdot) \triangleq p(y_{mt}|z_{mt}) = \mathcal{CN}(y_{mt}; z_{mt}, \sigma^2), \quad (15)$$

$$\begin{aligned} p(z_{mt}|\cdot) &\triangleq p(z_{mt}|\mathbf{g}_m^T, \mathbf{c}_t, \mathbf{h}_m^T, \mathbf{x}_t) \\ &= \delta(z_{mt} - \mathbf{g}_m^T \mathbf{c}_t - \mathbf{h}_m^T \mathbf{x}_t), \end{aligned} \quad (16)$$

$$p(c_{nt}|\cdot) \triangleq p(c_{nt}|\mathbf{f}_n^T, \mathbf{x}_t) = \delta(c_{nt} - s_{nt} \mathbf{f}_n^T \mathbf{x}_t). \quad (17)$$

The factorized distribution in (14) can be visualized by the factor graph shown in Fig. 2, which is divided into two sub-graphs, i.e., the left part and the right part. Therein, the variables $\{y_{mt}\}$, $\{z_{mt}\}$, $\{c_{nt}\}$, $\{g_{mn}\}$, $\{f_{nk}\}$, $\{h_{mk}\}$, and $\{x_{kt}\}$ are represented by the ‘‘variable nodes’’ that appear as hollow circles. The distributions $\{p(y_{mt}|\cdot)\}$, $\{p(z_{mt}|\cdot)\}$, $\{p(c_{nt}|\cdot)\}$, $\{p(g_{mn})\}$, $\{p(f_{nk})\}$, $\{p(h_{mk})\}$, and $\{p(x_{kt})\}$ are represented by the ‘‘factor nodes’’ that appear as black squares. Each variable node is connected to its associated factor nodes. In Fig. 2, the dashed blue lines exist only when the direct link exists.

B. Trilinear AMP Algorithm

A direct alternative of computing (11) is to use the canonical sum-product algorithm (SPA), which passes messages through the edges of the factor graph in Fig. 2. These messages describe the PDFs of the variables $\{z_{mt}\}$, $\{c_{nt}\}$, $\{g_{mn}\}$, $\{f_{nk}\}$, $\{h_{mk}\}$, and $\{x_{kt}\}$. However, exact inference using SPA remains intractable. To circumvent this, we resort to the AMP framework [23]–[25], [27] to approximately calculate (11). As a computationally efficient variant of SPA, the AMP algorithm has been applied successfully in many practical problems, such as RIS-based passive information transfer [12], [33] and conventional MIMO channel estimation [29], [34], [35].

In the algorithm derivation and later in the asymptotic performance analysis in Section V, we assume the following scaling conventions: the elements of \mathbf{F} and \mathbf{H} both scale as the order of $\mathcal{O}(1/\sqrt{K})$; the elements of \mathbf{G} scale as the order of $\mathcal{O}(1/\sqrt{N})$; the elements of \mathbf{X} and \mathbf{W} both scale as the order of $\mathcal{O}(1)$. As such, the elements of \mathbf{C} , $\mathbf{H}\mathbf{X}$, $\mathbf{G}\mathbf{C}$, and \mathbf{Z} scale as $\mathcal{O}(1)$, i.e., the same order as that of \mathbf{W} and \mathbf{X} .

Let us first provide an intuitive description of how the trilinear inference problem can be split into two bilinear inference problems. Based on (13), we rewrite (2) as

$$\mathbf{Y} = [\mathbf{G}, \mathbf{H}] [\mathbf{C}^T, \mathbf{X}^T]^T + \mathbf{W}, \quad (18)$$

$$\mathbf{C} = \mathbf{S} \odot \mathbf{F}\mathbf{X}. \quad (19)$$

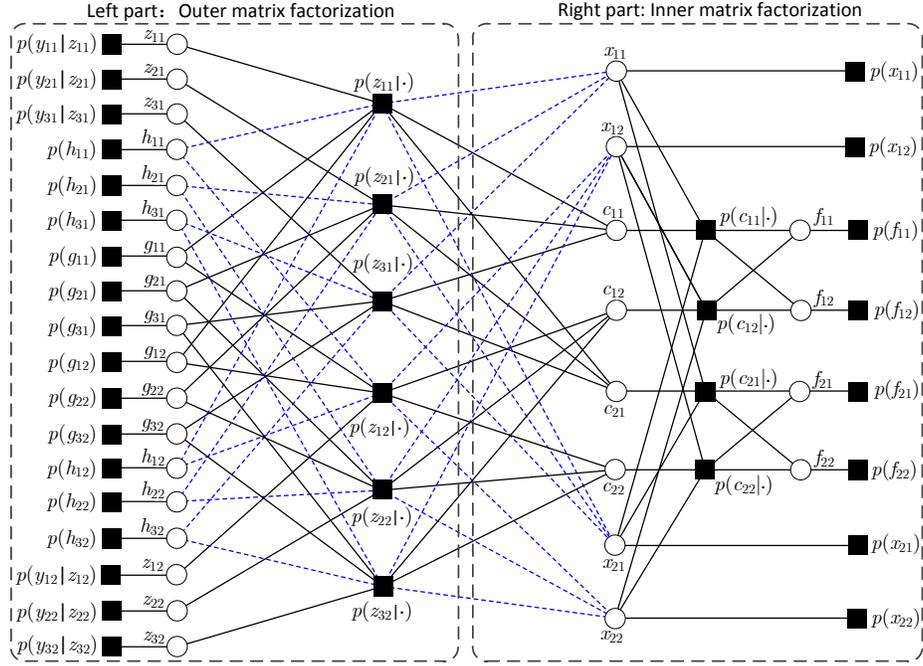


Fig. 2. The factor graph representation of (14) for a toy example with $M = 3$ and $N = T = K = 2$.

Clearly, inferring $[G, H]$ and $[C^\top, X^\top]^\top$ with noisy observation \mathbf{Y} in (18) and inferring \mathbf{F} and \mathbf{X} with missing observation \mathbf{C} in (19) are both bilinear matrix factorization problems. More specifically, the matrix factorization problem (19) is embedded into the matrix factorization problem (18). We henceforth refer the two matrix factorization problems in (19) and (18) to as the outer and inner matrix factorizations, which correspond to the left and right subgraphs in Fig. 2, respectively. Consequently, AMP over the two subgraphs can be performed by applying the BiG-AMP algorithm [25] alternatively. Messages are passed between the two subgraphs via the common variables \mathbf{C} and \mathbf{X} . As the entire iterative procedure is essentially solving the trilinear inference problem, we henceforth refer to it as the trilinear AMP (Tri-AMP) algorithm, which is summarized in Algorithm 1. In the following, we explain the steps of Algorithm 1 in detail from the outer matrix factorization (left part) to the inner matrix factorization (right part).

1) *Outer Matrix Factorization:* For the ease of notation, we drop the iteration index i in the following. The AMP over the left subgraph of Fig. 2 corresponds to Lines 3-13 of Algorithm 1. Specifically, Line 3 gives a “plug-in” estimate of each element z_{mt} of \mathbf{Z} and Line 5 applies “Onsager” correction to obtain the approximate Gaussian message with mean \hat{p}_{mt}

and variance v_{mt}^p by using the central-limit-theorem (CLT) argument. By taking the product of the incoming Gaussian message $\mathcal{CN}(z_{mt}; \hat{p}_{mt}, v_{mt}^p)$ and the likelihood $p(y_{mt}|z_{mt})$, the marginal posterior $p(z_{mt}|\hat{p}_{mt}, v_{mt}^p)$ is approximated by

$$p(z_{mt}|\hat{p}_{mt}, v_{mt}^p) \propto p(y_{mt}|z_{mt})\mathcal{CN}(z_{mt}; \hat{p}_{mt}, v_{mt}^p), \quad (20)$$

where $p(y_{mt}|z_{mt})$ is given in (15). The variance and mean of z_{mt} regarding to (20) in Line 6 of Algorithm 1 are computed as

$$v_{mt}^z = \frac{\sigma^2 v_{mt}^p}{\sigma^2 + v_{mt}^p} \quad (21)$$

$$\hat{z}_{mt} = \frac{\sigma^2 \hat{p}_{mt} + v_{mt}^p y_{mt}}{\sigma^2 + v_{mt}^p}, \quad (22)$$

respectively. The quantities v_{mt}^u and \hat{u}_{mt} updated in Line 7 are the equivalents of the Onsager correction of the scaled residual and the inverse residual variance, respectively. They are derived directly from the quadratic Gaussian approximations by second-order Taylor expansion. Using the CLT argument again, the updates in Line 8 correspond to the messages from the factor nodes (connected to c_{nt}) to the variable node c_{nt} except for the message from the factor node $p(c_{nt}|\mathbf{f}_n^\top, \mathbf{x}_t)$ to c_{nt} . The updates in Line 9 correspond to the messages from the factor nodes (connected to x_{kt}) to the variable node x_{kt} except

$$\begin{aligned} p(\mathbf{G}, \mathbf{F}, \mathbf{H}, \mathbf{X}, \mathbf{Z}, \mathbf{C}|\mathbf{Y}) &= \frac{1}{p(\mathbf{Y})} p(\mathbf{Y}|\mathbf{Z}) p(\mathbf{Z}|\mathbf{G}, \mathbf{C}, \mathbf{H}, \mathbf{X}) p(\mathbf{C}|\mathbf{F}, \mathbf{X}) p(\mathbf{G}) p(\mathbf{F}) p(\mathbf{H}) p(\mathbf{X}) \\ &= \frac{1}{p(\mathbf{Y})} \left(\prod_{m=1}^M \prod_{t=1}^T p(y_{mt}|z_{mt}) p(z_{mt}|\mathbf{g}_m^\top, \mathbf{c}_t, \mathbf{h}_m^\top, \mathbf{x}_t) \right) \left(\prod_{n=1}^N \prod_{t=1}^T p(c_{nt}|\mathbf{f}_n^\top, \mathbf{x}_t) \right) \left(\prod_{m=1}^M \prod_{n=1}^N p(g_{mn}) \right) \\ &\quad \times \left(\prod_{n=1}^N \prod_{k=1}^K p(f_{nk}) \right) \left(\prod_{m=1}^M \prod_{k=1}^K p(h_{mk}) \right) \left(\prod_{k=1}^K \prod_{t=1}^{T_p} p(x_{p,kt}) \right) \left(\prod_{k=1}^K \prod_{t=1}^{T_d} p(x_{d,kt}) \right), \end{aligned} \quad (14)$$

Algorithm 1: Tri-AMP Algorithm

Input: \mathbf{Y} , $\overline{\mathbf{X}}_p$, \mathbf{S} , σ^2 , prior distributions $p(\mathbf{G})$, $p(\mathbf{F})$, $p(\mathbf{H})$, and $p(\mathbf{X}_d)$

- 1: Initialization: $\forall m, n, k, t \in \{T_p + 1, \dots, T\}$: choose $\hat{g}_{mn}(1)$, $v_{mn}^g(1)$, $\hat{f}_{nk}(1)$, $v_{nk}^f(1)$, $\hat{h}_{mn}(1)$, $v_{mn}^h(1)$, $\hat{x}_{kt}(1)$, $v_{kt}^x(1)$; $\forall k, t \in \{1, \dots, T_p\}$: $\hat{x}_{kt}(1) = \overline{x}_{p,kt}$, $v_{kt}^x(1) = 0$; $\forall n, k, t$: $\hat{u}_{mt}(-1) = 0$, $\hat{\eta}_{nt}(-1) = 0$, $\hat{c}_{nt}(1) = s_{nt} \sum_{k=1}^K \hat{f}_{nk} \hat{x}_{kt}$, $v_{nt}^c(1) = s_{nt} \sum_{k=1}^K v_{nk}^f v_{kt}^x$
 - 2: **for** $i = 1, \dots, I_{\max}$
 - % Outer matrix factorization
 - 3: $\forall m, t$: $\bar{v}_{mt}^p(i) = \sum_{n=1}^N (|\hat{g}_{mn}(i)|^2 v_{nt}^c(i) + v_{mn}^g(i) |\hat{c}_{nt}(i)|^2) + \sum_{k=1}^K (|\hat{h}_{mk}(i)|^2 v_{kt}^x(i) + v_{mk}^h(i) |\hat{x}_{kt}(i)|^2)$
 - 4: $\forall m, t$: $\bar{p}_{mt}(i) = \sum_{n=1}^N \hat{g}_{mn}(i) \hat{c}_{nt}(i) + \sum_{k=1}^K \hat{h}_{mk}(i) \hat{x}_{kt}(i)$
 - 5: $\forall m, t$: $v_{mt}^p(i) = \bar{v}_{mt}^p(i) + \sum_{n=1}^N v_{mn}^g(i) v_{nt}^c(i) + \sum_{k=1}^K v_{mk}^h(i) v_{kt}^x(i)$, $\forall m, t$: $\hat{p}_{mt}(i) = \bar{p}_{mt}(i) - \hat{u}_{mt}(i-1) \bar{v}_{mt}^p(i)$
 - 6: $\forall m, t$: $v_{mt}^z(i) = \text{var}\{z_{mt} | \hat{p}_{mt}(i), v_{mt}^p(i)\}$, $\hat{z}_{mt}(i) = \mathbb{E}\{z_{mt} | \hat{p}_{mt}(i), v_{mt}^p(i)\}$
 - 7: $\forall m, t$: $v_{mt}^u(i) = (1 - v_{mt}^z(i)/v_{mt}^p(i))/v_{mt}^p(i)$, $\hat{u}_{mt}(i) = (\hat{z}_{mt}(i) - \hat{p}_{mt}(i))/v_{mt}^p(i)$
 - 8: $\forall n, t$: $v_{nt}^{rc}(i) = s_{nt} (\sum_{m=1}^M |\hat{g}_{mn}(i)|^2 v_{mt}^u(i))^{-1}$, $\hat{r}_{nt}^c(i) = s_{nt} (\hat{c}_{nt}(i) (1 - v_{nt}^{rc}(i) \sum_{m=1}^M v_{mn}^g(i) v_{mt}^u(i)) + v_{nt}^{rc}(i) \sum_{m=1}^M \hat{g}_{mn}^*(i) \hat{u}_{mt}(i))$
 - 9: $\forall k, t$: $v_{kt}^{rx}(i) = (\sum_{m=1}^M |\hat{h}_{mk}(i)|^2 v_{mt}^u(i))^{-1}$, $\hat{r}_{kt}^x(i) = \hat{x}_{kt}(i) (1 - v_{kt}^{rx}(i) \sum_{m=1}^M v_{mk}^h(i) v_{mt}^u(i)) + v_{kt}^{rx}(i) \sum_{m=1}^M \hat{h}_{mk}^*(i) \hat{u}_{mt}(i)$
 - 10: $\forall m, n$: $v_{mn}^{gg}(i) = (\sum_{t=1}^T |\hat{c}_{nt}(i)|^2 v_{mt}^u(i))^{-1}$, $\hat{q}_{mn}^g(i) = \hat{g}_{mn}(i) (1 - v_{mn}^{gg}(i) \sum_{t=1}^T v_{nt}^c(i) v_{mt}^u(i)) + v_{mn}^{gg}(i) \sum_{t=1}^T \hat{c}_{nt}^*(i) \hat{u}_{mt}(i)$
 - 11: $\forall m, k$: $v_{mk}^{gh}(i) = (\sum_{t=1}^T |\hat{x}_{kt}(i)|^2 v_{mt}^u(i))^{-1}$, $\hat{q}_{mk}^h(i) = \hat{h}_{mk}(i) (1 - v_{mk}^{gh}(i) \sum_{t=1}^T v_{kt}^x(i) v_{mt}^u(i)) + v_{mk}^{gh}(i) \sum_{t=1}^T \hat{x}_{kt}^*(i) \hat{u}_{mt}(i)$
 - 12: $\forall m, n$: $v_{mn}^g(i+1) = \text{var}\{g_{mn} | \hat{q}_{mn}^g(i), v_{mn}^{gg}(i)\}$, $\hat{g}_{mn}(i+1) = \mathbb{E}\{g_{mn} | \hat{q}_{mn}^g(i), v_{mn}^{gg}(i)\}$
 - 13: $\forall m, k$: $v_{mk}^h(i+1) = \text{var}\{h_{mk} | \hat{q}_{mk}^h(i), v_{mk}^{gh}(i)\}$, $\hat{h}_{mk}(i+1) = \mathbb{E}\{h_{mk} | \hat{q}_{mk}^h(i), v_{mk}^{gh}(i)\}$
 - % Inner matrix factorization
 - 14: $\forall n, t$: $\tilde{v}_{nt}^p(i) = \sum_{k=1}^K |\hat{f}_{nk}(i)|^2 v_{kt}^x(i) + v_{nk}^f(i) |\hat{x}_{kt}(i)|^2$, $\tilde{p}_{nt}(i) = \sum_{k=1}^K \hat{f}_{nk}(i) \hat{x}_{kt}(i)$
 - 15: $\forall n, t$: $v_{nt}^\xi(i) = \tilde{v}_{nt}^p(i) + \sum_{k=1}^K v_{nk}^f(i) v_{kt}^x(i)$, $\hat{\xi}_{nt}(i) = \tilde{p}_{nt}(i) - \hat{\eta}_{nt}(i-1) \tilde{v}_{nt}^p(i)$
 - 16: $\forall n, t$: $v_{nt}^c(i) = s_{nt} \text{var}\{c_{nt} | \hat{r}_{nt}^c(i), v_{nt}^{rc}(i), \hat{\xi}_{nt}(i), v_{nt}^\xi(i)\}$, $\hat{c}_{nt}(i) = s_{nt} \mathbb{E}\{c_{nt} | \hat{r}_{nt}^c(i), v_{nt}^{rc}(i), \hat{\xi}_{nt}(i), v_{nt}^\xi(i)\}$
 - 17: $\forall n, t$: $v_{nt}^\eta(i) = s_{nt} (1 - v_{nt}^c(i)/v_{nt}^\xi(i))/v_{nt}^\xi(i)$, $\hat{\eta}_{nt}(i) = s_{nt} (\hat{c}_{nt}(i) - \hat{\xi}_{nt}(i))/v_{nt}^\xi(i)$
 - 18: $\forall k, t$: $v_{kt}^\gamma(i) = (\sum_{n=1}^N |\hat{f}_{nk}(i)|^2 v_{nt}^\eta(i))^{-1}$, $\hat{\gamma}_{kt}(i) = \hat{x}_{kt}(i) (1 - v_{kt}^\gamma(i) \sum_{n=1}^N v_{nk}^f(i) v_{nt}^\eta(i)) + v_{kt}^\gamma(i) \sum_{n=1}^N \hat{f}_{nk}^*(i) \hat{\eta}_{nt}(i)$
 - 19: $\forall n, k$: $v_{nk}^{ff}(i) = (\sum_{t=1}^T |\hat{x}_{kt}(i)|^2 v_{nt}^\eta(i))^{-1}$, $\hat{q}_{nk}^f(i) = \hat{f}_{nk}(i) (1 - v_{nk}^{ff}(i) \sum_{t=1}^T v_{kt}^x(i) v_{nt}^\eta(i)) + v_{nk}^{ff}(i) \sum_{t=1}^T \hat{x}_{kt}^*(i) v_{nt}^\eta(i)$
 - 20: $\forall n, k$: $\hat{f}_{nk}(i+1) = \mathbb{E}\{f_{nk} | \hat{q}_{nk}^f(i), v_{nk}^{ff}(i)\}$, $v_{nk}^f(i+1) = \text{var}\{f_{nk} | \hat{q}_{nk}^f(i), v_{nk}^{ff}(i)\}$
 - 21: $\forall k, t \in \{T_p + 1, \dots, T\}$: $v_{kt}^x(i+1) = \text{var}\{x_{kt} | \hat{r}_{kt}^x(i), \hat{\gamma}_{kt}(i), v_{kt}^{rx}(i), v_{kt}^\gamma(i)\}$, $\hat{x}_{kt}(i+1) = \mathbb{E}\{x_{kt} | \hat{r}_{kt}^x(i), \hat{\gamma}_{kt}(i), v_{kt}^{rx}(i), v_{kt}^\gamma(i)\}$
 - 22: $\forall k, t \in \{1, \dots, T_p\}$: $v_{kt}^x(i+1) = 0$, $\hat{x}_{kt}(i+1) = \overline{x}_{p,kt}$
 - 23: **if** a certain stopping criterion is met, **stop**
 - 24: **end for**
- Output:** $\hat{\mathbf{G}}$, $\hat{\mathbf{F}}$, $\hat{\mathbf{H}}$, and $\hat{\mathbf{X}}$
-

for the message from the prior $p(x_{kt})$. By taking the product of all incoming messages at the variable nodes $\{g_{mn}\}$ and $\{h_{mk}\}$, we arrive at the updates of g_{mn} and h_{mk} (Lines 12 and 13) with respect to the marginal posterior distributions

$$p(g_{mn} | \hat{q}_{mn}^g, v_{mn}^{gg}) \propto p(g_{mn}) \mathcal{CN}(g_{mn}; \hat{q}_{mn}^g, v_{mn}^{gg}), \quad (23)$$

$$p(h_{mk} | \hat{q}_{mk}^h, v_{mk}^{gh}(i)) \propto p(h_{mk}) \mathcal{CN}(h_{mk}; \hat{q}_{mk}^h, v_{mk}^{gh}), \quad (24)$$

respectively, where $\mathcal{CN}(g_{mn}; \hat{q}_{mn}^g, v_{mn}^{gg})$ and $\mathcal{CN}(h_{mk}; \hat{q}_{mk}^h, v_{mk}^{gh})$ are the messages (Lines 10 and 11) from all the factor nodes $\{p(z_{mt} | \mathbf{g}_m^\top, \mathbf{c}_t, \mathbf{h}_m^\top, \mathbf{x}_t)\}_{1 \leq t \leq T}$ to the variable node g_{mn} and to the variable node h_{mk} , respectively.

2) *Inner Matrix Factorization:* The AMP updates over the right part subgraph of Fig. 2 (i.e., Lines 14-22 of Algorithm 1) is similar to that of the outer matrix factorization. The differences between them lie in the updates of the posterior means and variances of c_{nt} and x_{kt} , which correspond to Line 16 and Lines 21-22, respectively. Specifically, the updates of the mean and variance of c_{nt} combine the support information of s_{nt} . The detailed calculations in Line 16 are based on the marginal posterior distribution

$$p(c_{nt} | \hat{r}_{nt}^c, v_{nt}^{rc}, \hat{\xi}_{nt}, v_{nt}^\xi) \propto p(c_{nt} | \hat{r}_{nt}^c, v_{nt}^{rc}) \mathcal{CN}(c_{nt}; \hat{\xi}_{nt}, v_{nt}^\xi),$$

where $p(c_{nt} | \hat{r}_{nt}^c, v_{nt}^{rc})$ is given by

$$p(c_{nt} | \hat{r}_{nt}^c, v_{nt}^{rc}) = \begin{cases} \mathcal{CN}(c_{nt}; \hat{r}_{nt}^c, v_{nt}^{rc}), & s_{nt} = 1 \\ \delta(c_{nt}), & s_{nt} = 0 \end{cases}. \quad (25)$$

The updates of the mean and variance of x_{kt} combine the Gaussian message $\mathcal{CN}(x_{kt}; \hat{r}_{kt}^x, v_{kt}^x)$ in Line 9 of Algorithm 1 from the left part subgraph. Taking the product of all the incoming messages at the variable node x_{kt} yields the updates in Lines 21 and 22 of Algorithm 1 with respect to the marginal posterior distribution

$$\begin{aligned} & p(x_{kt} | \hat{r}_{kt}^x, \hat{\gamma}_{kt}^x, v_{kt}^{rx}, v_{kt}^\gamma) \\ & \propto p(x_{kt}) \mathcal{CN}(x_{kt}; \hat{r}_{kt}^x, v_{kt}^{rx}) \mathcal{CN}(x_{kt}; \hat{\gamma}_{kt}^x, v_{kt}^\gamma) \\ & \propto p(x_{kt}) \mathcal{CN}\left(x_{kt}; \frac{v_{kt}^{rx} \hat{\gamma}_{kt}^x + v_{kt}^\gamma \hat{r}_{kt}^x}{v_{kt}^{rx} + v_{kt}^\gamma}, \frac{v_{kt}^{rx} + v_{kt}^\gamma}{v_{kt}^{rx} + v_{kt}^\gamma}\right), \end{aligned} \quad (26)$$

where $\mathcal{CN}(x_{kt}; \hat{\gamma}_{kt}^x, v_{kt}^\gamma)$ is the approximated Gaussian message obtained from $p(c_{nt} | \mathbf{f}_n^\top, \mathbf{x}_t)$ to x_{kt} by employing the CLT argument. As the first T_p columns of \mathbf{X} are used as pilots, i.e., $\mathbf{X}_p = \overline{\mathbf{X}}_p$, where $\overline{\mathbf{X}}_p$ is the *known* pilot matrix, from (5) and (7) we have

$$p(x_{kt}) = \delta(x_{kt} - \overline{x}_{p,kt}), t \in \{1, \dots, T_p\}. \quad (27)$$

Substituting (27) into (26) yields the posterior mean and variance of x_{kt} as follows

$$\hat{x}_{kt} = \mathbb{E}\{x_{kt} | \hat{r}_{kt}^x, \hat{\gamma}_{kt}^x, v_{kt}^{rx}, v_{kt}^{\gamma x}\} = \bar{x}_{p,kt}, \quad (28)$$

$$v_{kt}^x = \text{var}\{x_{kt} | \hat{r}_{kt}^x, \hat{\gamma}_{kt}^x, v_{kt}^{rx}, v_{kt}^{\gamma x}\} = 0, \quad (29)$$

which corresponds to the update in Line 22 of Algorithm 1.

Algorithm 1 can be extended to the case where the direct link is absent, i.e., $\mathbf{H} = \mathbf{0}$ and the dashed blue lines in Fig. 2 do not exist. Due to limited space, we omit the algorithmic details in this case.

C. Damping

The approximations used in Tri-AMP are justified only in the large system limit. In other words, the approximated messages might not come close to Gaussian distributions in practice, particularly with the finite dimensions of M, N, K, T_p, T_d . In this case, the Tri-AMP algorithm appears to have some unexpected numerical issues and diverges. This is also observed in other AMP-based algorithms [18], [25]. In this paper, we use the damping method to improve the numerical robustness of Tri-AMP. Specifically, in each iteration we smoothen the updates of the variances and means of $\mathbf{G}, \mathbf{F}, \mathbf{H}$, and \mathbf{X} by using a convex combination with the current and previous updates. For example, the updates in Line 12 of Algorithm 1 are replaced by

$$v_{mn}^g(i+1) \triangleq (1-\beta)v_{mn}^g(i) + \beta v_{mn}^g(i+1), \quad (30)$$

$$\hat{g}_{mn}(i+1) \triangleq (1-\beta)\hat{g}_{mn}(i) + \beta\hat{g}_{mn}(i+1), \quad (31)$$

where $\beta \in [0, 1]$ is the damping factor. Our experiments under Rayleigh fading channels and QPSK/Gaussian signals suggest that choosing β within $[0.1, 0.2]$ leads to a good performance. The damping operation in Lines 12, 13, 20, and 21 in Algorithm 1 can be replaced in a similar way.

D. Computational Complexity

We now briefly discuss the computational complexity of the Tri-AMP algorithm. Note that the total computational complexity of Tri-AMP is due to the computation in both the outer matrix factorization and the inner matrix factorization. We thus sketch the respective complexity as follows. First, the complexity of the outer matrix factorization requires $\mathcal{O}(M(N+K)T)$ flops per iteration. Second, the complexity of the inner matrix factorization requires $\mathcal{O}(NKT)$ flops per iteration. Consequently, the total complexity of Tri-AMP is at most $I_{\max}(\mathcal{O}(M(N+K)T) + \mathcal{O}(NKT))$ flops, where I_{\max} is the maximum number of iterations required in Tri-AMP. When the direct link is absent, i.e., $\mathbf{H} = \mathbf{0}$, the total computational complexity of the corresponding algorithm is at most $I_{\max}(\mathcal{O}(M(N)T) + \mathcal{O}(NKT))$.

V. ASYMPTOTIC PERFORMANCE ANALYSIS

The previous section presents an AMP-based iterative algorithm to approximately calculate the posterior mean estimators in (11). However, it is unclear whether the proposed algorithm can approach the theoretical MSEs in (12), which are generally difficult to evaluate. To this end, we use the *replica method* [26] to evaluate the asymptotic performance of the MSEs (12) in the

large-system limit. Note that despite not being mathematically rigorous, the replica method has proven successful in analysing the asymptotic performance of the bilinear inference problems [27], [29] and the matrix calibration inference problems [18]. In this section, we generalize the analytical results in [29] to the trilinear inference problem (2), which includes the bilinear inference problem in [29] as a special case when the user-RIS-BS link is absent. Specifically, we shall illustrate that the MSEs (12) asymptotically converge to the MSEs of scalar additive white Gaussian noise (AWGN) channels with tractable expressions.

Our asymptotic analysis is carried out under the large-system limit, i.e., M, N, K, T_p, T_d with the ratios $M/K, N/K, T_p/K, T_d/K$ being fixed and finite. For simplicity, we utilize $K \rightarrow \infty$ to denote this large-system limit. In addition, we assume that the elements of $\mathbf{H}, \mathbf{G}, \mathbf{F}, \mathbf{X}$, and \mathbf{W} are all i.i.d. variables, and scale as the same orders as those in Section IV B. The analytical result is elaborated in Proposition 1 of Section V-B. Before proceeding to the main result, we first introduce preliminaries involved in the main result.

A. Preliminaries

Similarly to (5), we partition \mathbf{C} and \mathbf{Z} respectively as

$$\mathbf{C} \triangleq [\mathbf{C}_p, \mathbf{C}_d] \text{ with } \mathbf{C}_p \in \mathbb{C}^{N \times T_p} \text{ and } \mathbf{C}_d \in \mathbb{C}^{N \times T_d}, \quad (32)$$

$$\mathbf{Z} \triangleq [\mathbf{Z}_p, \mathbf{Z}_d] \text{ with } \mathbf{Z}_p \in \mathbb{C}^{M \times T_p} \text{ and } \mathbf{Z}_d \in \mathbb{C}^{M \times T_d}. \quad (33)$$

To facilitate the analysis, we define the second-order moments:

$$q_g \triangleq \mathbb{E}\{|g_{mn}|^2\}, q_h \triangleq \mathbb{E}\{|h_{mk}|^2\}, q_f \triangleq \mathbb{E}\{|f_{nk}|^2\}, \quad (34a)$$

$$q_{x_p} \triangleq \mathbb{E}\{|x_{p,kt}|^2\}, q_{c_p} \triangleq \mathbb{E}\{|c_{p,nt}|^2\} = \rho K q_f q_{x_p}, \quad (34b)$$

$$q_{x_d} \triangleq \mathbb{E}\{|x_{d,kt}|^2\}, q_{c_d} \triangleq \mathbb{E}\{|c_{d,nt}|^2\} = \rho K q_f q_{x_d}, \quad (34c)$$

where the expectations are taken over the prior distributions in (3) and (4). Moreover, we define the following scalar AWGN channels:

$$y_g \triangleq \sqrt{\tilde{m}_g} g + w_g, y_f \triangleq \sqrt{\tilde{m}_f} f + w_f, \quad (35a)$$

$$y_h \triangleq \sqrt{\tilde{m}_h} h + w_h, y_{x_d} \triangleq \sqrt{\tilde{m}_{x_d}} x_d + w_{x_d}, \quad (35b)$$

where $\{w_h, w_g, w_f, w_{x_d}\} \sim \mathcal{CN}(\cdot; 0, 1)$, $g \sim p(g_{mn})$, $f \sim p(f_{nk})$, $h \sim p(h_{mk})$, $x_d \sim p(x_{d,kt})$. The parameters $\{\tilde{m}_g, \tilde{m}_f, \tilde{m}_h, \tilde{m}_{x_d}\}$ will be specified later in (42). By Bayes' theorem, for given $\{\tilde{m}_g, \tilde{m}_f, \tilde{m}_h, \tilde{m}_{x_d}\}$, we attain the following posterior distributions:

$$p(g|y_g) \propto p(y_g|g) p(g_{mn}), p(f|y_f) \propto p(y_f|f) p(f_{nk}),$$

$$p(h|y_h) \propto p(y_h|h) p(h_{mk}), p(x_d|y_{x_d}) \propto p(y_{x_d}|x_d) p(x_{d,kt}),$$

where $p(y_g|g) = \mathcal{CN}(y_g; \sqrt{\tilde{m}_g} g, 1)$, $p(y_f|f) = \mathcal{CN}(y_f; \sqrt{\tilde{m}_f} f, 1)$, $p(y_h|h) = \mathcal{CN}(y_h; \sqrt{\tilde{m}_h} h, 1)$, and $p(y_{x_d}|x_d) = \mathcal{CN}(y_{x_d}; \sqrt{\tilde{m}_{x_d}} x_d, 1)$.

The posterior mean estimators of g, f, h , and x_d with respect to the scalar AWGN channels in (35) are given by

$$\hat{g} = \int p(g|y_g) g dg, \hat{f} = \int p(f|y_f) f df \quad (37a)$$

$$\hat{h} = \int p(h|y_h) h dh, \hat{x}_d = \int p(x_d|y_{x_d}) x_d dx_d. \quad (37b)$$

Consequently, the MSEs of the estimators in (37) are given by

$$\text{MSE}_g = \mathbb{E}_{g,y_g} \{|g - \hat{g}|^2\}, \quad (38)$$

$$\text{MSE}_f = \mathbb{E}_{f,y_f} \{|f - \hat{f}|^2\}, \quad (39)$$

$$\text{MSE}_h = \mathbb{E}_{h,y_h} \{|h - \hat{h}|^2\}, \quad (40)$$

$$\text{MSE}_{x_d} = \mathbb{E}_{x_d,y_{x_d}} \{|x_d - \hat{x}_d|^2\}. \quad (41)$$

B. Main Result

Under some commonly used assumptions in the replica analysis, we have the following large-system limit performance on the MSEs in 12 of the considered channel estimation problem.

Proposition 1: By replica method, when $K \rightarrow \infty$, $\{\text{MSE}_G, \text{MSE}_F, \text{MSE}_H, \text{MSE}_{X_d}\}$ converges to $\{\text{MSE}_g, \text{MSE}_f, \text{MSE}_h, \text{MSE}_{x_d}\}$ that corresponds to a fixed-point solution of (38)–(41) and the following equations:

$$m_g = q_g - \text{MSE}_g, \tilde{m}_g = \rho T_p m_{c_p} a_p + \rho T_d m_{c_d} a_d, \quad (42a)$$

$$m_f = q_f - \text{MSE}_f, \tilde{m}_f = T_p q_{x_p} b_p + T_d m_{x_d} b_d, \quad (42b)$$

$$m_h = q_h - \text{MSE}_h, \tilde{m}_h = T_p q_{x_p} a_p + T_d m_{x_d} a_d, \quad (42c)$$

$$m_{x_d} = q_{x_d} - \text{MSE}_{x_d}, \tilde{m}_{x_d} = N m_f b_d + M m_h a_d, \quad (42d)$$

where

$$a_p = \frac{1}{\sigma^2 + \rho N(q_g q_{c_p} - m_g m_{c_p}) + K q_{x_p}(q_h - m_h)}, \quad (43a)$$

$$a_d = \frac{1}{\sigma^2 + \rho N(q_g q_{c_d} - m_g m_{c_d}) + K(q_h q_{x_d} - m_h m_{x_d})}, \quad (43b)$$

$$b_p = \frac{\rho}{1/(M m_g a_p) + K q_{x_p}(q_f - m_f)}, \quad (43c)$$

$$b_d = \frac{\rho}{1/(M m_g a_d) + K(q_f q_{x_d} - m_f m_{x_d})}, \quad (43d)$$

$$m_{c_o} = q_{c_o} - \frac{K(q_{x_o} q_f - m_{x_o} m_f)}{1 + M K m_g a_o (q_{x_o} q_f - m_{x_o} m_f)}. \quad (43e)$$

Herein, $o \in \{p, d\}$; q_g, q_f, q_h, q_{x_o} , and q_{c_o} are defined in (34).

Proof: See Appendix A. ■

It follows from Proposition 1 that the fixed-point of (38)–(42) asymptotically describes the MSEs in (12). The fixed-point solution can be efficiently calculated by an iterative algorithm that sequentially updates $\{\text{MSE}_i, \tilde{m}_i, m_i, i \in \{g, f, h, x_d\}\}$ via (38)–(42) until convergence.

Note that Proposition 1 deals with asymptotic MSEs in the general case where the user-RIS-BS link and the user-BS link are both present, i.e. $\mathbf{G} \neq \mathbf{0}$, $\mathbf{F} \neq \mathbf{0}$, and $\mathbf{H} \neq \mathbf{0}$. Nevertheless, the analysis can be applied to cases where some of channel links are missing. As shown in the subsequent corollaries, the cases in the absence of the user-BS, user-RIS and/or RIS-BS channels are special cases of Proposition 1.

Corollary 1: By replica method, when the user-BS channel is absent ($\mathbf{H} = \mathbf{0}$) and $K \rightarrow \infty$, $\{\text{MSE}_G, \text{MSE}_F, \text{MSE}_{X_d}\}$ converges to $\{\text{MSE}_g, \text{MSE}_f, \text{MSE}_{x_d}\}$ that corresponds to a fixed-point solution of (38), (39), (41), and the following equations:

$$m_g = q_g - \text{MSE}_g, \tilde{m}_g = \rho T_p m_{c_p} a_p + \rho T_d m_{c_d} a_d, \quad (44a)$$

$$m_f = q_f - \text{MSE}_f, \tilde{m}_f = T_p q_{x_p} b_p + T_d m_{x_d} b_d, \quad (44b)$$

$$m_{x_d} = q_{x_d} - \text{MSE}_{x_d}, \tilde{m}_{x_d} = N m_f b_d, \quad (44c)$$

where

$$a_p = \frac{1}{\sigma^2 + \rho N(q_g q_{c_p} - m_g m_{c_p})}, \quad (45a)$$

$$a_d = \frac{1}{\sigma^2 + \rho N(q_g q_{c_d} - m_g m_{c_d})}, \quad (45b)$$

$$b_p = \frac{\rho}{1/(M m_g a_p) + K q_{x_p}(q_f - m_f)}, \quad (45c)$$

$$b_d = \frac{\rho}{1/(M m_g a_d) + K(q_f q_{x_d} - m_f m_{x_d})}. \quad (45d)$$

Herein, m_{c_o} ($o \in \{p, d\}$) is given in (43e); q_g, q_f, q_{x_o} , and q_{c_o} are defined in (34).

Proof: Since $\mathbf{H} = \mathbf{0}$, we obtain $h \sim p(h_{mk}) = \delta(h_{mk})$ and $q_h = m_h = \text{MSE}_h = 0$ in (42) and (43), which leads to Corollary 1. ■

Corollary 2: By replica method, when the user-RIS and/or RIS-BS channels are absent ($\mathbf{G} = \mathbf{0}$ and/or $\mathbf{F} = \mathbf{0}$) and $K \rightarrow \infty$, $\{\text{MSE}_H, \text{MSE}_{X_d}\}$ converges to $\{\text{MSE}_h, \text{MSE}_{x_d}\}$ that corresponds to a fixed-point solution of (40), (41), and the following equations:

$$m_h = q_h - \text{MSE}_h,$$

$$\tilde{m}_h = \frac{T_p q_{x_p}}{\sigma^2 + K q_{x_p}(q_h - m_h)} + \frac{T_d m_{x_d}}{\sigma^2 + K(q_h q_{x_d} - m_h m_{x_d})},$$

$$m_{x_d} = q_{x_d} - \text{MSE}_{x_d},$$

$$\tilde{m}_{x_d} = \frac{M m_h}{\sigma^2 + K(q_h q_{x_d} - m_h m_{x_d})}.$$

Herein, q_h and q_{x_o} ($o \in \{p, d\}$) are defined in (34).

Proof: Since $\mathbf{G} = \mathbf{0}$ and/or $\mathbf{F} = \mathbf{0}$, we have $p(g) \sim p(g_{mn}) = \delta(g_{mn})$ and/or $p(f) \sim p(f_{nk}) = \delta(f_{nk})$, and thus $q_g = m_g = \text{MSE}_g = q_f = m_f = \text{MSE}_f = m_{c_p} = q_{c_p} = m_{c_d} = q_{c_d} = 0$ in (42) and (43), which leads to Corollary 2. ■

We note that the analytical result in Corollary 2 agrees with the result in conventional massive MIMO systems reported in [29, Propostion 1].

C. Case Study: Rayleigh Fading Channels and QPSK Signals

The final expressions of the asymptotic MSEs derived in Section V-B depends on the exact forms of the prior distributions $p(g_{mn})$, $p(f_{nk})$, $p(h_{mk})$, and $p(x_{kt})$. We can simplify the integrals involved in (38)–(41) into closed-form expressions once the associated prior distributions are specified. To illustrate this, we focus on a concrete case with Rayleigh fading channels and QPSK signals. That is, we set $p(g_{mn}) = \mathcal{CN}(g_{mn}; 0, q_g)$, $p(f_{nk}) = \mathcal{CN}(f_{nk}; 0, q_f)$, and $p(h_{mk}) = \mathcal{CN}(h_{mk}; 0, q_h)$. The training signal \mathbf{X}_p and the data signal \mathbf{X}_d are both drawn both from a QPSK constellation with unit variance and equal probabilities.

By substituting the prior distributions specified above into (38)–(41), we attain

$$\text{MSE}_g = \frac{q_g}{1 + q_g \tilde{m}_g}, \quad (47)$$

$$\text{MSE}_f = \frac{q_f}{1 + q_f \tilde{m}_f}, \quad (48)$$

$$\text{MSE}_h = \frac{q_h}{1 + q_h \tilde{m}_h}, \quad (49)$$

$$\text{MSE}_{x_d} = 1 - \int D\zeta \tanh(\tilde{m}_{x_d} + \sqrt{\tilde{m}_{x_d}}\zeta), \quad (50)$$

where $D\zeta = \frac{1}{\sqrt{2\pi}}e^{-\zeta^2/2}d\zeta$ is a Gaussian integration measure. By evaluating the second scalar AWGN channel in (35b) according to [36, Page 269], the asymptotic symbol error rate (SER) of \mathbf{X}_d is given as

$$\text{SER} = 2Q(\sqrt{\tilde{m}_{x_d}}) - \left(Q(\sqrt{\tilde{m}_{x_d}})\right)^2 \quad (51)$$

where $Q(x) = \int_x^\infty D\zeta$ is the Q-function.

VI. NUMERICAL STUDIES

This section conducts numerical experiments to corroborate the semi-blind channel estimation performance of the proposed Tri-AMP algorithm in a RIS-aided massive MIMO system. The user-RIS channel matrix \mathbf{F} , the RIS-BS channel matrix \mathbf{G} , and the user-BS channel matrix \mathbf{H} (when the direct link exists, i.e., $\mathbf{H} \neq \mathbf{0}$) are generated from the i.i.d. Gaussian distribution with unit variance. Each entry of the payload data \mathbf{X} is generated from the i.i.d. QPSK constellation with transmit power 1. We adopt the asymptotic analytical result shown in Proposition 1 as a benchmark to validate the performance of the Tri-AMP algorithm.² All the simulation results are obtained by averaging 2,000 independent trials unless otherwise specified. The signal-to-noise ratio (SNR) is defined as

$$\begin{aligned} \text{SNR} &= \frac{\sum_{t=1}^T \mathbb{E} \left\{ \left\| \mathbf{G}(\mathbf{s}^{(t)} \odot (\mathbf{F}\mathbf{x}^{(t)})) + \mathbf{H}\mathbf{x}^{(t)} \right\|_2^2 \right\}}{T\sigma^2} \\ &= \frac{\rho N K \tau_g \tau_f \tau_x + K \tau_h \tau_x}{\sigma^2}, \end{aligned} \quad (52)$$

where τ_g , τ_f , τ_h , and τ_x are the variances of \mathbf{G} , \mathbf{F} , \mathbf{H} , and \mathbf{X} , respectively. We choose MSE³ as the performance metric of the estimates of \mathbf{G} , \mathbf{F} , and \mathbf{H} , and SER as the performance metric of the detection of the QPSK signal \mathbf{X}_d .

A. Under i.i.d. Rayleigh Fading Channels

We consider the setup under $M = 256$, $N = 128$, and $K = 20$. A baseline method, referred to as BiGAMP+LMMSE, is adopted for comparison. Similarly to the two-stage approach in [15] where the direct link is absent, the BiGAMP+LMMSE is conducted in two separate stages: the first stage uses the BiGAMP algorithm to obtain the estimates of \mathbf{G} , \mathbf{H} , and \mathbf{X}_d ; the second stage uses the estimated \mathbf{X}_d and the linear minimum mean square error (LMMSE) approach to calculate the estimate of \mathbf{F} . Beside this, the JBF-MC [15], the methods in [16] and [19], and the PARAFAC [20] are included for comparison.

To test the minimum number of pilots required for respective algorithms, we first consider the case without noise, i.e., $\sigma^2 = 0$. We say that it is successful if all the MSEs of \mathbf{G} , \mathbf{F} , and \mathbf{H} are less than -60 dB and the SER of \mathbf{X}_d is

²Although the replica analysis in Section V is valid only in the large-system limit, we adopt the derived asymptotic MSE bound as a benchmark for finite-size systems considered in simulations. More specifically, we take the settings used in simulation to determine the values of m/K , N/K , T_p/K , T_d/K , and then apply Proposition 1 with these ratios to determine the performance bound of the replica method.

³The MSEs in the simulations are defined similarly to (12) by replacing the expectation with the sample average over the number of independent trials.

TABLE I
MINIMUM TRAINING LENGTH T_p OF RESPECTIVE ALGORITHMS VERSUS T
WITH $\sigma^2 = 0$, $M = 256$, $N = 128$, $K = 20$, AND $\rho = 0.3$

Algorithm \ T	100	300	500	1000	2000	3000
Tri-AMP	✗	25	22	20	20	20
BiGAMP+LMMSE	✗	✗	160	150	146	140
JBF-MC [15]	✗	✗	465	465	465	465
Method in [16]	✗	167	167	167	167	167
Method in [19]	✗	✗	✗	✗	✗	2580
PARAFAC [20]	✗	✗	✗	800	800	800
Replica Result	✗	0	0	0	0	0

^a “✗” indicates that the corresponding scheme is infeasible even when $T_p = T$.

^b Here “0” in the replica result means that, under the specified parameter ratios, the asymptotic MSEs of \mathbf{G} , \mathbf{F} , \mathbf{H} in the large system limit can be reduced to less than -60 dB even without the use of any pilot symbols. It is worth noting that the trilinear estimation problem with zero pilots suffer from the phase and permutation ambiguities in the factorization of $\mathbf{F}\mathbf{X}$; see the detailed discussions on the phase and permutation ambiguities [35]. The Bayesian inference (and so the replica method) cannot resolve these ambiguities. Additional pilot symbols are required if one needs to resolve these ambiguities [35].

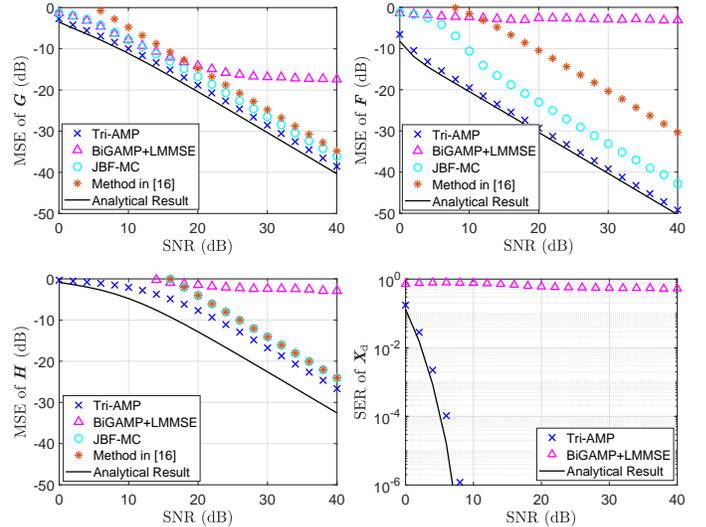


Fig. 3. MSEs of \mathbf{G} , \mathbf{F} , and \mathbf{H} , and SER of \mathbf{X}_d versus the SNR with $M = 256$, $N = 128$, $K = 20$, $\rho = 0.3$, $T_p = 90$, and $T = 300$.

zero. The minimum training length of the pilots of various algorithms under different block lengths T is listed in Table I by averaging 200 trials. We see that the Tri-AMP algorithm requires only about 20 pilots when $T \geq 200$, which is much smaller than the other baseline approaches. In particular, all the associated schemes including the replica result are infeasible when $T = 100$.

We now consider the noisy case and set $\rho = 0.3$ except for the phase diagram test and set $T = 300$. The methods in [16] and [19] are not included as it fails in the case of $T_p < 300$ (see Table I). The MSEs of \mathbf{G} , \mathbf{F} , and \mathbf{H} , and the SER of \mathbf{X}_d versus the SNR are depicted in Fig. 3 with $T_p = 90$ and $T = 300$. The

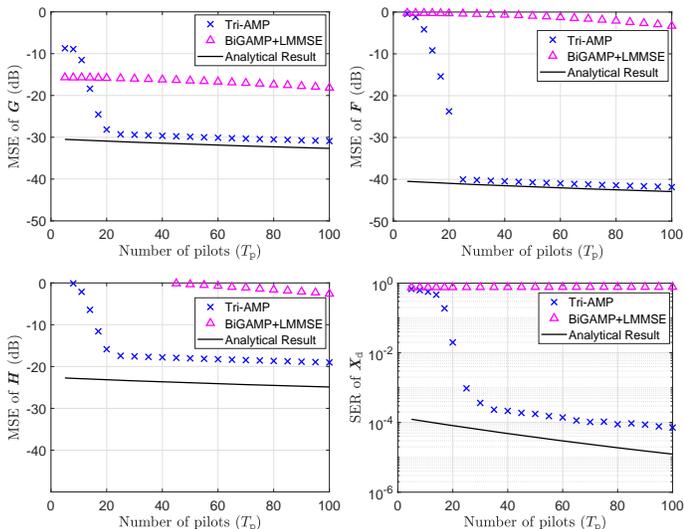


Fig. 4. MSEs of \mathbf{G} , \mathbf{F} , and \mathbf{H} , and SER of \mathbf{X}_d versus the number of pilots T_p with $M = 256$, $N = 128$, $K = 20$, $\rho = 0.3$, and $T_d = 300$.

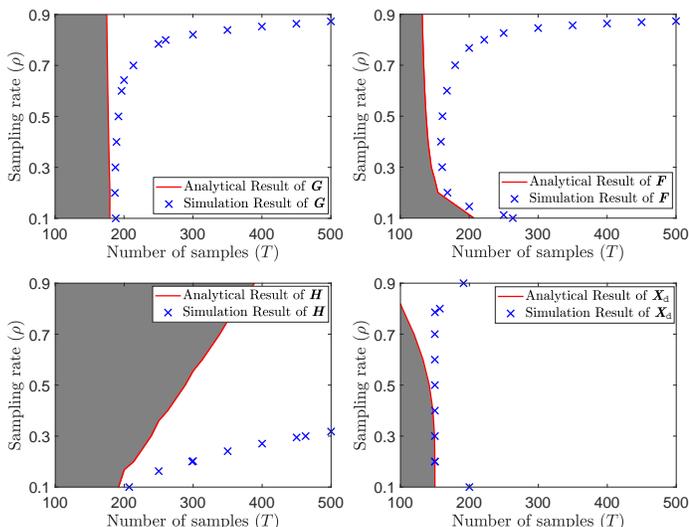


Fig. 5. Phase diagrams of \mathbf{G} , \mathbf{F} , \mathbf{H} , and \mathbf{X}_d versus the sampling rate ρ and the number of samples T with $M = 256$, $N = 128$, $K = 20$, $\rho = 0.3$, and $T_p = 90$, SNR = 30 dB.

MSEs of \mathbf{G} , \mathbf{F} , and \mathbf{H} with SNR = 30 dB, and the SER of \mathbf{X}_d with SNR = 5 dB versus the number of pilots are depicted in Fig. 4. As seen from Figs. 3 and 4, the performance of Tri-AMP is consistently superior to BiGAMP+LMMSE. The MSEs of \mathbf{G} and \mathbf{F} are very close to the analytical results. Nevertheless, there exists a gap of about 3 dB gap between the analytical result and the simulation result with respect to the estimate of \mathbf{H} . We conjecture that this is because the proposed message-passing algorithm perform well in sparse matrix factorization.

Fig. 5 depicts the phase diagrams with a varying value of the sampling rate ρ and the number of samples (T). The boundary of the phase diagram in MSEs of \mathbf{G} , \mathbf{F} , and \mathbf{H} denotes the case with MSE = -20 dB and the gray region of the analytical result represents the region where MSE < -20 dB. Likewise, the boundary of the phase diagram in evaluating the detection performance of \mathbf{X}_d denotes the case with SER = 10^{-4} . We see that the simulation results of Tri-AMP are close to the analytical performance bound when ρ is relatively low but not too low.

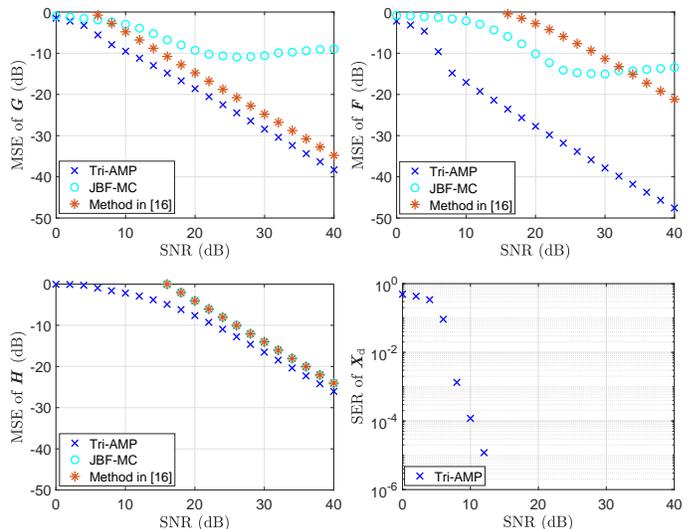


Fig. 6. MSEs of \mathbf{G} , \mathbf{F} , and \mathbf{H} , and SER of \mathbf{X}_d versus the SNR. $M = 256$, $N = 128$, $K = 20$, $\rho = 0.3$, $T_p = 90$, and $T = 300$.

Especially, the sparsity level ρ of the on-off matrix \mathbf{S} is set between 0.2 and 0.4 to achieve a good estimation performance of the proposed Tri-AMP algorithm.

B. Under Correlated Rayleigh Fading Channels

We next consider the simulation tests under the correlated Rayleigh fading channel model. We follow [16], [37] to construct a correlated channel model where the channel correlation matrix is an exponential matrix. Specifically, the channel matrices \mathbf{G} , \mathbf{F} , and \mathbf{H} are modeled as

$$\mathbf{G} = \overline{\mathbf{C}}_g \overline{\mathbf{G}}, \mathbf{F} = \overline{\mathbf{C}}_f \overline{\mathbf{F}}, \mathbf{H} = \overline{\mathbf{C}}_h \overline{\mathbf{H}}, \quad (53)$$

respectively, where $\overline{\mathbf{G}}$, $\overline{\mathbf{F}}$, and $\overline{\mathbf{H}}$ are i.i.d. Rayleigh fading channels and

$$[\overline{\mathbf{C}}_g]_{i,j} = c_g^{(i-j)}, [\overline{\mathbf{C}}_f]_{i,j} = c_f^{(i-j)}, [\overline{\mathbf{C}}_h]_{i,j} = c_h^{(i-j)} \quad (54)$$

for $i > j$, where $|c_g| < 1$, $|c_f| < 1$, $|c_h| < 1$, $[\mathbf{C}_g]_{i,j} = [\mathbf{C}_g]_{j,i}^*$, $[\mathbf{C}_f]_{i,j} = [\mathbf{C}_f]_{j,i}^*$, $[\mathbf{C}_h]_{i,j} = [\mathbf{C}_h]_{j,i}^*$. We set the correlation coefficients c_g , c_f , c_h to be $0.2 + 0.6j$, $0.4 + 0.3j$, $0.5 + 0.1j$, respectively. Fig. 6 depicts the MSEs of \mathbf{G} , \mathbf{F} , and \mathbf{H} , and the SER of \mathbf{X}_d versus the SNR while keeping the same setup as that of Fig. 3 except for the channel model. We see that the Tri-AMP algorithm bears a similar performance as that of Fig. 3 and still outperforms all baseline methods.

We now consider the setup with SNR = 40 dB and relatively large transmission blocks of $T = 1000, 2000, 3000$. Except for T and T_p , the other parameter settings are the same as those of Fig. 6. Tri-AMP use only $T_p = 100$ pilots in the transmission frame, whereas all the baseline methods use the whole transmission frame as pilots. The corresponding MSEs of \mathbf{G} , \mathbf{F} , and \mathbf{H} are shown in Table II. We observe that even using only 100 pilots, the proposed Tri-AMP algorithm still present a decent performance improvement over the baseline methods, where all baseline methods use the whole transmission block as pilots.

VII. CONCLUSIONS

We have considered the problem of semi-blind cascaded channel estimation in RIS-aided massive MIMO systems. We

TABLE II

AVERAGE MSE COMPARISON OF VARIOUS ALGORITHMS WITH VARYING BLOCK LENGTH T , $T_p = 100$ FOR TRI-AMP, AND $T_p = T$ FOR BASELINE METHODS. $M = 256$, $N = 128$, $K = 20$, AND $\rho = 0.3$.

Algorithm	T			
	MSE	1000	2000	3000
Tri-AMP	MSE _g (dB)	-46.39	-49.71	-51.55
	MSE _f (dB)	-57.62	-60.87	-62.98
	MSE _h (dB)	-34.34	-37.72	-39.48
JBF-MC [15]	MSE _g (dB)	-33.55	-44.38	-46.78
	MSE _f (dB)	-43.99	-53.76	-56.35
	MSE _h (dB)	-24.05	-24.05	-24.05
Method in [16]	MSE _g (dB)	-39.48	-41.51	-42.42
	MSE _f (dB)	-22.25	-22.47	-22.58
	MSE _h (dB)	-24.05	-24.06	-24.06
Method in [19]	MSE _g (dB)	\mathcal{X}	\mathcal{X}	-40.25
	MSE _f (dB)	\mathcal{X}	\mathcal{X}	-20.56
	MSE _h (dB)	\mathcal{X}	\mathcal{X}	-23.55
PARAFAC [20]	MSE _g (dB)	-36.33	-41.08	-42.96
	MSE _f (dB)	-3.56	-10.44	-15.14
	MSE _h (dB)	-24.05	-24.05	-24.05

“ \mathcal{X} ” indicates that the corresponding scheme is infeasible.

formulated the semi-blind cascaded channel estimation problem as a trilinear estimation problem under the Bayesian MMSE inference framework. We have developed a computationally efficient AMP algorithm to iteratively calculate the marginal posterior distributions. We have also derived the analytical MSE performance based on the replica method in the large-system limit. We provided experimental evidences to demonstrate that the proposed algorithm achieves an accurate channel estimation with a small number of pilot overhead.

APPENDIX A PROOF OF PROPOSITION 1

Based on the argument in [27], as $K \rightarrow \infty$, the MSEs in (12) converge to a stationary point of the average free energy

$$\mathcal{F} \triangleq \lim_{K \rightarrow \infty} \frac{1}{K^2} \mathbb{E}_{\mathbf{Y}} [\ln p(\mathbf{Y})], \quad (55)$$

where $p(\mathbf{Y}) = \int_{\mathbf{G}, \mathbf{F}, \mathbf{H}, \mathbf{X}, \mathbf{Z}, \mathbf{C}} p(\mathbf{Y}, \mathbf{G}, \mathbf{F}, \mathbf{H}, \mathbf{X}, \mathbf{Z}, \mathbf{C})$ is the partition function. Note that directly evaluating $\mathbb{E}_{\mathbf{Y}} [\ln p(\mathbf{Y})]$ in 55 is intractable. We sidestep this issue by applying $\mathbb{E}[\ln x] = \lim_{n \rightarrow 0} \frac{\partial}{\partial n} \ln \mathbb{E}[x^n]$ in (55) to transform the expectation inside the log-function, and obtain

$$\mathcal{F} = \lim_{K \rightarrow \infty} \frac{1}{K^2} \lim_{\tau \rightarrow 0} \frac{\partial}{\partial \tau} \ln \mathbb{E}_{\mathbf{Y}} [p^\tau(\mathbf{Y})], \quad (56)$$

where $p^\tau(\mathbf{Y})$ denotes τ identical replicas of $p(\mathbf{Y})$. To proceed with the calculation of \mathcal{F} , the following assumption commonly used in the replica method is made:

Assumption 1: The order of the two limits $\tau \rightarrow 0$ and $K \rightarrow \infty$ in (56) can be exchanged without affecting the final result.

Under *Assumption 1*, the calculation of \mathcal{F} in (56) becomes

$$\mathcal{F} = \lim_{\tau \rightarrow 0} \frac{\partial}{\partial \tau} \lim_{K \rightarrow \infty} \frac{1}{K^2} \ln \mathbb{E}_{\mathbf{Y}} [p^\tau(\mathbf{Y})]. \quad (57)$$

It turns out that we first needs to compute the analytical expression of

$$\lim_{K \rightarrow \infty} \frac{1}{K^2} \ln \mathbb{E}_{\mathbf{Y}} [p^\tau(\mathbf{Y})], \quad (58)$$

which can be obtained by using Varadhan’s theorem [38, Appendix I], as will be detailed in the following.

For an integer τ , we denote the a -th replica of the user-BS channel matrix \mathbf{H} , $0 \leq a \leq \tau$, by $\mathbf{H}^{(a)}$, which follows the same distribution as \mathbf{H} .⁴ We further define the collection of all the $\tau + 1$ replicas of \mathbf{H} as $\mathcal{H} \triangleq [\text{vec}(\mathbf{H}^{(0)}), \dots, \text{vec}(\mathbf{H}^{(\tau)})] \in \mathbb{C}^{MK \times (\tau+1)}$, where $\text{vec}(\cdot)$ is the vectorization operator. Likewise, we define the collections of the $\tau + 1$ replicas of \mathbf{G} , \mathbf{F} , \mathbf{X}_o , \mathbf{C}_o , and \mathbf{Z}_o as \mathcal{G} , \mathcal{F} , \mathcal{X}_o , \mathcal{C}_o , and \mathcal{Z}_o , $o \in \{\text{p}, \text{d}\}$, respectively. With these definitions, we express $\mathbb{E}_{\mathbf{Y}} [p^\tau(\mathbf{Y})]$ as

$$\mathbb{E}_{\mathbf{Y}} [p^\tau(\mathbf{Y})] = \mathbb{E}_{\mathcal{A}} \left[\int d\mathbf{Y} \prod_{a=0}^{\tau} p(\mathbf{Y} | \mathbf{Z}^{(a)}) \right], \quad (59)$$

where $\mathcal{A} \triangleq \{\mathcal{H}, \mathcal{G}, \mathcal{F}, \mathcal{X}_o, \mathcal{C}_o, \mathcal{Z}_o\}$. To average over $p(\mathcal{A})$ in the right hand side (RHS) of (59), we introduce six $(\tau+1) \times (\tau+1)$ auxiliary matrices $\mathbf{Q}_h \triangleq [Q_h^{ab}]$, $\mathbf{Q}_g \triangleq [Q_g^{ab}]$, $\mathbf{Q}_f \triangleq [Q_f^{ab}]$, $\mathbf{Q}_{x_o} \triangleq [Q_{x_o}^{ab}]$, $\mathbf{Q}_{c_o} \triangleq [Q_{c_o}^{ab}]$, and $\mathbf{Q}_{z_o} \triangleq [Q_{z_o}^{ab}]$, whose elements are defined by

$$\begin{aligned} Q_h^{ab} &\triangleq \frac{1}{MK} \sum_{mk} (h_{mk}^{(a)})^* h_{mk}^{(b)}, & Q_g^{ab} &\triangleq \frac{1}{MN} \sum_{mn} (g_{mn}^{(a)})^* g_{mn}^{(b)}, \\ Q_f^{ab} &\triangleq \frac{1}{NK} \sum_{nk} (f_{nk}^{(a)})^* f_{nk}^{(b)}, & Q_{x_o}^{ab} &\triangleq \frac{1}{KT_o} \sum_{kt} (x_{o,kt}^{(a)})^* x_{o,kt}^{(b)}, \\ Q_{c_o}^{ab} &\triangleq \frac{1}{NT_o} \sum_{kt} (c_{o,kt}^{(a)})^* c_{o,kt}^{(b)}, \end{aligned} \quad (60)$$

respectively, where $0 \leq a, b \leq \tau$ and $o \in \{\text{p}, \text{d}\}$. By Bayes’ theorem and inserting the equivalent Dirac’s delta expressions of Q_h^{ab} , Q_g^{ab} , Q_f^{ab} , $Q_{x_o}^{ab}$, and $Q_{c_o}^{ab}$ into the RHS of (59), i.e.,

$$\begin{aligned} 1 &= MK \int \prod_{0 \leq a \leq b}^{\tau} \delta \left(\sum_{mk} (h_{mk}^{(a)})^* h_{mk}^{(b)} - MK Q_h^{ab} \right) dQ_h^{ab}, \\ 1 &= MN \int \prod_{0 \leq a \leq b}^{\tau} \delta \left(\sum_{mn} (g_{mn}^{(a)})^* g_{mn}^{(b)} - MN Q_g^{ab} \right) dQ_g^{ab}, \\ 1 &= NK \int \prod_{0 \leq a \leq b}^{\tau} \delta \left(\sum_{nk} (f_{nk}^{(a)})^* f_{nk}^{(b)} - NK Q_f^{ab} \right) dQ_f^{ab}, \\ 1 &= KT_o \int \prod_{0 \leq a \leq b}^{\tau} \delta \left(\sum_{kt} (x_{o,nt}^{(a)})^* x_{o,nt}^{(b)} - KT_o Q_{x_o}^{ab} \right) dQ_{x_o}^{ab}, \\ 1 &= MT_o \int \prod_{0 \leq a \leq b}^{\tau} \delta \left(\sum_{nt} (c_{o,nt}^{(a)})^* c_{o,nt}^{(b)} - MT_o Q_{c_o}^{ab} \right) dQ_{c_o}^{ab}, \end{aligned}$$

and by performing the integrals with a change of variables from \mathcal{A} to $\{\mathbf{Q}_h, \mathbf{Q}_g, \mathbf{Q}_f, \mathbf{Q}_{x_o}, \mathbf{Q}_{c_o}, \mathbf{Q}_{z_o}\}$, we obtain $\mathbb{E}_{\mathbf{Y}} [p^\tau(\mathbf{Y})]$ in (61), shown at the bottom of the next page, where

$$p(\mathbf{Q}_h) = \mathbb{E}_{\mathcal{H}} \left\{ \prod_{0 \leq a \leq b}^{\tau} \delta \left(\sum_{mk} (h_{mk}^{(a)})^* h_{mk}^{(b)} - MK Q_h^{ab} \right) \right\},$$

⁴For the ease of notation, we define $\mathbf{H}^{(0)} \triangleq \mathbf{H}$.

$$p(\mathbf{Q}_g) = \mathbb{E}_{\mathcal{G}} \left\{ \prod_{0 \leq a \leq b}^{\tau} \delta \left(\sum_{mn} \left(g_{mn}^{(a)} \right)^* g_{mn}^{(b)} - MN Q_g^{ab} \right) \right\},$$

$$p(\mathbf{Q}_f) = \mathbb{E}_{\mathcal{F}} \left\{ \prod_{0 \leq a \leq b}^{\tau} \delta \left(\sum_{nk} \left(f_{nk}^{(a)} \right)^* f_{nk}^{(b)} - NK Q_f^{ab} \right) \right\},$$

$$p(\mathbf{Q}_{x_p}, \mathbf{Q}_{x_d}) = \mathbb{E}_{\mathcal{X}_p, \mathcal{X}_d} \left\{ \prod_{o \in \{p, d\}} \prod_{0 \leq a \leq b}^{\tau} \delta \left(\sum_{kt} \left(x_{o, kt}^{(a)} \right)^* x_{o, kt}^{(b)} - KT_o Q_{x_o}^{ab} \right) \right\},$$

$$p(\mathbf{Q}_{c_p}, \mathbf{Q}_{c_d}) = \mathbb{E}_{\mathcal{C}_p, \mathcal{C}_d} \left\{ \prod_{o \in \{p, d\}} \prod_{0 \leq a \leq b}^{\tau} \delta \left(\sum_{nt} \left(c_{o, nt}^{(a)} \right)^* c_{o, nt}^{(b)} - NT_o Q_{c_o}^{ab} \right) \right\}.$$

As Q_h^{ab} , Q_g^{ab} , Q_f^{ab} , and $Q_{x_o}^{ab}$ consists of the summations of i.i.d. random variables, it follows from the Cramer theorem that the probability measures $p(\mathbf{Q}_h)$, $p(\mathbf{Q}_g)$, $p(\mathbf{Q}_f)$, $p(\mathbf{Q}_{x_p}, \mathbf{Q}_{x_d})$ satisfy the large derivation theory (LDT) and can be written as

$$p(\mathbf{Q}_h) = e^{-MK\mathcal{R}(\mathbf{Q}_h) + o(MK)}, \quad (63)$$

$$p(\mathbf{Q}_g) = e^{-MN\mathcal{R}(\mathbf{Q}_g) + o(MN)}, \quad (64)$$

$$p(\mathbf{Q}_f) = e^{-NK\mathcal{R}(\mathbf{Q}_f) + o(NK)}, \quad (65)$$

$$p(\mathbf{Q}_{x_p}, \mathbf{Q}_{x_d}) = e^{-KT\mathcal{R}(\mathbf{Q}_{x_p}, \mathbf{Q}_{x_d}) + o(KT)}, \quad (66)$$

where $o(MK)$ stands for any correction term in the sense that $\lim_{K \rightarrow \infty} \frac{o(MK)}{MK} = 0$, $\mathcal{R}(\mathbf{Q}_h)$, $\mathcal{R}(\mathbf{Q}_g)$, $\mathcal{R}(\mathbf{Q}_f)$, and $\mathcal{R}(\mathbf{Q}_{x_p}, \mathbf{Q}_{x_d})$ are the corresponding rate functions. By the Legendre-Fenchel transform [38, eqs. (129) and (130)] of the scaled cumulant generating functions of \mathbf{Q}_h , \mathbf{Q}_g , \mathbf{Q}_f , \mathbf{Q}_{x_o} , these rate functions in (63)–(73) can be expressed as

$$\mathcal{R}(\mathbf{Q}_h) = \inf_{\tilde{\mathbf{Q}}_h} \{\mathcal{I}_h\}, \quad \mathcal{R}(\mathbf{Q}_g) = \inf_{\tilde{\mathbf{Q}}_g} \{\mathcal{I}_g\}, \quad (67)$$

$$\mathcal{R}(\mathbf{Q}_f) = \inf_{\tilde{\mathbf{Q}}_f} \{\mathcal{I}_f\}, \quad \mathcal{R}(\mathbf{Q}_{x_p}, \mathbf{Q}_{x_d}) = \inf_{\tilde{\mathbf{Q}}_{x_p}, \tilde{\mathbf{Q}}_{x_d}} \{\mathcal{I}_x\}, \quad (68)$$

where $\tilde{\mathbf{Q}}_h$, $\tilde{\mathbf{Q}}_g$, $\tilde{\mathbf{Q}}_f$, and $\tilde{\mathbf{Q}}_{x_o}$, $o \in \{p, d\}$ are $(\tau + 1) \times (\tau + 1)$ auxiliary matrices which can be viewed as the dual variables of \mathbf{Q}_h , \mathbf{Q}_g , \mathbf{Q}_f , and \mathbf{Q}_{x_o} , $o \in \{p, d\}$, respectively, and

$$\mathcal{I}_h = \lim_{K \rightarrow \infty} \frac{1}{MK} \ln \mathbb{E}_{\mathcal{H}} \left\{ e^{\text{tr}(\tilde{\mathbf{Q}}_h \mathcal{H}^H \mathcal{H})} \right\} - \text{tr}(\tilde{\mathbf{Q}}_h \mathbf{Q}_h), \quad (69)$$

$$\mathcal{I}_g = \lim_{K \rightarrow \infty} \frac{1}{MN} \ln \mathbb{E}_{\mathcal{G}} \left\{ e^{\text{tr}(\tilde{\mathbf{Q}}_g \mathcal{G}^H \mathcal{G})} \right\} - \text{tr}(\tilde{\mathbf{Q}}_g \mathbf{Q}_g), \quad (70)$$

$$\mathcal{I}_f = \lim_{K \rightarrow \infty} \frac{1}{NK} \ln \mathbb{E}_{\mathcal{F}} \left\{ e^{\text{tr}(\tilde{\mathbf{Q}}_f \mathcal{F}^H \mathcal{F})} \right\} - \text{tr}(\tilde{\mathbf{Q}}_f \mathbf{Q}_f), \quad (71)$$

$$\mathcal{I}_x = \sum_{o \in \{p, d\}} \lim_{K \rightarrow \infty} \frac{1}{KT_o} \left(\ln \mathbb{E}_{\mathcal{X}} \left\{ e^{\text{tr}(\tilde{\mathbf{Q}}_{x_o} \mathcal{X}_o^H \mathcal{X}_o)} \right\} - \text{tr}(\tilde{\mathbf{Q}}_{x_o} \mathbf{Q}_{x_o}) \right), \quad (72)$$

Note that $\mathbf{C}^{(a)} = \mathbf{S} \odot (\mathbf{F}^{(a)} \mathbf{X}^{(a)})$ and the elements of $\mathbf{C}^{(a)}$ are not i.i.d. variables and hence the Cramer theorem cannot be applied for $\mathbf{Q}_c^{(ab)}$. To deal with this, we apply Gärtner-Ellis Theorem [39, Chapter 2.3] which is suitable for proving the

LDT property of the averaging of non i.i.d. variables. That is, $\mathbf{Q}_c^{(ab)}$ still satisfies the LTD property and the probability measure $p(\mathbf{Q}_{c_p}, \mathbf{Q}_{c_d})$ can be expressed as

$$p(\mathbf{Q}_{c_p}, \mathbf{Q}_{c_d}) = e^{-NT\mathcal{R}(\mathbf{Q}_{c_p}, \mathbf{Q}_{c_d}) + o(NT)}, \quad (73)$$

with the rate function $\mathcal{R}(\mathbf{Q}_{c_p}, \mathbf{Q}_{c_d})$ being as

$$\mathcal{R}(\mathbf{Q}_{c_p}, \mathbf{Q}_{c_d}) = \inf_{\tilde{\mathbf{Q}}_{c_p}, \tilde{\mathbf{Q}}_{c_d}} \{\mathcal{I}_c\}, \quad (74)$$

where

$$\mathcal{I}_c = \sum_{o \in \{p, d\}} \left(\lim_{K \rightarrow \infty} \frac{1}{NT_o} \ln \mathbb{E}_{\mathcal{C}} \left\{ e^{\text{tr}(\tilde{\mathbf{Q}}_{c_o} \mathcal{C}_o^H \mathcal{C}_o)} \right\} - \text{tr}(\tilde{\mathbf{Q}}_{c_o} \mathbf{Q}_{c_o}) \right). \quad (75)$$

where the expectation is with respect to the conditional probability density $p(\{c_{nt}^{(a)}\}_{0 \leq a \leq \tau}; \mathbf{Q}_{x_p}, \mathbf{Q}_{x_d}, \mathbf{Q}_f)$ given in (62).

Plugging (63)–(73) into (61) and using the Varadhan's theorem [39, Chapter 2.4] and [38, Appendix I]. (also called the saddle-point method) and ignoring the correction terms as $K \rightarrow \infty$ yields

$$\lim_{K \rightarrow \infty} \frac{1}{K^2} \ln \mathbb{E}_{\mathbf{Y}} \{p^\tau(\mathbf{Y})\} = \sup_{\{\mathbf{Q}_i\}} \inf_{\{\tilde{\mathbf{Q}}_i\}} \mathcal{F}(\tau) = \text{extr}_{\{\mathbf{Q}_i, \tilde{\mathbf{Q}}_i\}} \mathcal{F}(\tau) \quad (76)$$

where $i \in \{h, g, f, x_p, x_d, c_p, c_d\}$, 'extr' denotes the operation of extremization,

$$\mathcal{F}(\tau) \triangleq \left(\frac{MT_o}{K^2} \mathcal{I}_z + \frac{M}{K} \mathcal{I}_h + \frac{MN}{K^2} \mathcal{I}_g + \frac{N}{M} \mathcal{I}_f + \frac{T_o}{K} \mathcal{I}_x + \frac{NT_o}{K^2} \mathcal{I}_c \right), \quad (77)$$

and

$$\mathcal{I}_z = \sum_{o \in \{p, d\}} \ln \mathbb{E}_{\{z_{nt}^{(a)}\} | \mathbf{Q}_z} \left\{ \int dy \prod_{a=0}^n \mathcal{CN}(y; z_o^{(a)}, \sigma^2) \right\}, \quad (78)$$

where the expectation is with respect to

$$p(\{z_{nt}^{(a)}\}_{0 \leq a \leq n} | \mathbf{Q}_z) = \begin{cases} \mathcal{CN}(\{z_{nt}^{(a)}\}; \mathbf{0}, \mathbf{Q}_{z_d}), 1 \leq t \leq T_p, \\ \mathcal{CN}(\{z_{nt}^{(a)}\}; \mathbf{0}, \mathbf{Q}_{z_d}), T_p + 1 \leq t \leq T, \end{cases}$$

where $\mathbf{Q}_{c_o} = [\rho K Q_f^{ab} Q_{x_o}^{ab}]_{0 \leq a, b \leq n}$ and $\mathbf{Q}_{z_o} = [K Q_h^{ab} Q_{x_o}^{ab} + N Q_g^{ab} Q_{c_o}^{ab}]_{0 \leq a, b \leq n}$ for $o \in \{p, d\}$.

With (76), the average free energy \mathcal{F} in (57) becomes

$$\mathcal{F} = \lim_{\tau \rightarrow 0} \frac{\partial}{\partial \tau} \text{extr}_{\{\mathbf{Q}_i, \tilde{\mathbf{Q}}_i\}} \mathcal{F}(\tau), \quad (79)$$

which implies that the key is to obtain an analytic expression of (76). However, it is still prohibitive to get explicit expressions about the saddle points by setting zero gradient of $\mathcal{F}(\tau)$ with respect to $\{\mathbf{Q}_i, \tilde{\mathbf{Q}}_i\}$. For the sake of analytical tractability, we adopt the following replica symmetric ansatz:

Assumption 2: The saddle points of $\{\mathbf{Q}_i, \tilde{\mathbf{Q}}_i\}$ of $\mathcal{F}(\tau)$ fol-

low the replica symmetric forms, i.e.,

$$\mathbf{Q}_i = (q_i - m_i)\mathbf{I} + m_i\mathbf{1}\mathbf{1}^\top \quad (80)$$

$$\tilde{\mathbf{Q}}_i = (\tilde{q}_i - \tilde{m}_i)\mathbf{I} + \tilde{m}_i\mathbf{1}\mathbf{1}^\top \quad (81)$$

where $i \in \{h, g, f, x_p, x_d\}$, \mathbf{I} and $\mathbf{1}$ denotes the $(\tau+1) \times (\tau+1)$ identity matrix and the $(\tau+1)$ column vector with all elements being 1, respectively.

The above replica symmetric assumption implies that \mathbf{Q}_{z_o} and \mathbf{Q}_{c_o} also have a symmetric structure. Substituting (80) and (81) into (77), we have

$$\mathcal{F} = \lim_{\tau \rightarrow 0} \frac{\partial}{\partial \tau} \text{extr}_{\{q_i, m_i, \tilde{q}_i, \tilde{m}_i\}} \mathcal{F}(\tau), \quad (82)$$

where $i \in \{h, g, f, x_p, x_d, c_p, c_d\}$. As such, the extermination with respect to $\{\mathbf{Q}_i, \tilde{\mathbf{Q}}_i\}$ in (79) is reduced to those with respect to $\{q_i, m_i, \tilde{q}_i, \tilde{m}_i\}$ in (82).

Now, we compute the final expression of $\mathcal{F}(\tau)$ in (77) under Assumption 2. It suffices to simplify $\mathcal{I}_z, \mathcal{I}_h, \mathcal{I}_g, \mathcal{I}_f, \mathcal{I}_x,$ and \mathcal{I}_c . By plugging (80) and (81) into (78) and using the Hubbard-Stratonovich transform⁵, we simplify \mathcal{I}_z in (78) as

$$\mathcal{I}_z = 2M \sum_{o \in \{p, d\}} T_o \ln \mathbb{E}_{v, u', y} \left\{ \mathbb{E}_u^\tau \left\{ \mathcal{N}(y; c_{o,1}u + c_{o,2}v; \sigma^2) \right\} \right\}, \quad (83)$$

where $c_{o,1} = \sqrt{q_{z_o} - m_{z_o}}$, $c_{o,2} = \sqrt{m_{z_o}}$, $y \sim \mathcal{N}(y; c_{o,1}u' + c_{o,2}v, \sigma^2)$, $v, u', u \sim \mathcal{N}(\cdot; 0, 1)$. Similarly, the expression of \mathcal{I}_h in (69) can be simplified as (84), shown at the bottom of this page, where $h, h' \sim p(h_{mk})$. The simplified expressions of $\mathcal{I}_g, \mathcal{I}_f, \mathcal{I}_x,$ and \mathcal{I}_c under Assumption 2 are similar to (84) and are omitted here for brevity.

With (82) and (83), we compute the extremum of $\mathcal{F}(\tau)$ with respect to $\{q_i, m_i, \tilde{q}_i, \tilde{m}_i\}$, which can be obtained by setting the partial derivatives of $\mathcal{F}(\tau)$ to zero. Noting that $\lim_{\tau \rightarrow 0} \mathbb{E}_Y \{p^\tau(\mathbf{Y})\} = 1$, we find $\tilde{q}_i = 0$ and q_i satisfies (34). Note that the replica value of τ is an integer. In order to take the derivative of $\text{extr} \mathcal{F}(\tau)$ with respect to τ and the limit $\tau \rightarrow 0$ in (82), we need another replica assumption

Assumption 3: The function $\mathcal{F}(\tau)$ in (77) has analytic continuation with respect to real τ .

Under Assumption 3, by taking the derivative of $\text{extr} \mathcal{F}(\tau)$ with respect to τ and letting $\tau \rightarrow 0$, we obtain the analytical expression of \mathcal{F} in (85) where h, h', v, u, u' are defined in and (83) and (84); $g, g' \sim p(g_{mn})$; $f, f' \sim p(f_{nk})$; $x_o, x'_o \sim p(x_{o,kt})$. By computing the stationary point of \mathcal{F} in (85) with

⁵For $\zeta > 0$ and $x \in \mathbb{R}$, $e^{x^2} = \sqrt{\frac{\zeta}{2\pi}} \int_{\eta} e^{-\frac{\zeta}{2}\eta^2 + \sqrt{2\zeta}x\eta}$

respect to $\{q_i, m_i, \tilde{q}_i, \tilde{m}_i\}$, we obtain the asymptotic MSEs of (12), as desired in Proposition 1.

REFERENCES

- [1] E. G. Larsson, O. Edfors, F. Tufvesson, and T. L. Marzetta, "Massive MIMO for next generation wireless systems," *IEEE Commun. Mag.*, vol. 52, no. 2, pp. 186–195, Feb. 2014.
- [2] Huawei, "Huawei launches 5g simplified solution," [Online]. Available: <https://www.huawei.com/en/press-events/news/2019/2/huawei-5g-simplified-solution>, Feb. 2019.
- [3] E. Björnson, L. Sanguinetti, H. Wymeersch, J. Hoydis, and T. L. Marzetta, "Massive MIMO is a reality—what is next?: Five promising research directions for antenna arrays," *Digital Signal Process.*, vol. 94, pp. 3–20, Nov. 2019.
- [4] C. Huang, A. Zappone, G. C. Alexandropoulos, M. Debbah, and C. Yuen, "Reconfigurable intelligent surfaces for energy efficiency in wireless communication," *IEEE Trans. Wireless Commun.*, vol. 18, no. 8, pp. 4157–4170, Aug. 2019.
- [5] E. Basar, M. Di Renzo, J. De Rosny, M. Debbah, M.-S. Alouini, and R. Zhang, "Wireless communications through reconfigurable intelligent surfaces," *IEEE Access*, vol. 7, pp. 116 753–116 773, 2019.
- [6] M. Di Renzo, A. Zappone, M. Debbah, M.-S. Alouini, C. Yuen, J. de Rosny, and S. Tretyakov, "Smart radio environments empowered by reconfigurable intelligent surfaces: How it works, state of research, and road ahead," *arXiv preprint arXiv:2004.09352*, 2020.
- [7] Q. Wu and R. Zhang, "Intelligent reflecting surface enhanced wireless network via joint active and passive beamforming," *IEEE Trans. Wireless Commun.*, vol. 18, no. 11, pp. 5394–5409, Nov. 2019.
- [8] T. J. Cui, M. Q. Qi, X. Wan, J. Zhao, and Q. Cheng, "Coding metamaterials, digital metamaterials and programmable metamaterials," *Light: Science & Applications*, vol. 3, no. 10, pp. e218–e218, 2014.
- [9] Y.-C. Liang, R. Long, Q. Zhang, J. Chen, H. V. Cheng, and H. Guo, "Large intelligent surface/antennas (LISA): Making reflective radios smart," *J. Commun. Netw.*, vol. 4, no. 2, pp. 40–50, Jun. 2019.
- [10] C. Liaskos, S. Nie, A. Tsioliaridou, A. Pitsillides, S. Ioannidis, and I. Akyildiz, "A new wireless communication paradigm through software-controlled metasurfaces," *IEEE Commun. Mag.*, vol. 56, no. 9, pp. 162–169, Sep. 2018.
- [11] M. Di Renzo, M. Debbah, D.-T. Phan-Huy, A. Zappone, M.-S. Alouini, C. Yuen, V. Sciancalepore, G. C. Alexandropoulos, J. Hoydis, H. Gacanin, J. Rosny, A. Bounceu, G. Lerosey, and M. Fink, "Smart radio environments empowered by reconfigurable AI meta-surfaces: An idea whose time has come," *EURASIP J. Wireless Commun.*, no. 129, pp. 1–20, May 2019.
- [12] W. Yan, X. Kuai, and X. Yuan, "Passive beamforming and information transfer via large intelligent metasurface," *IEEE Wireless Commun. Lett.*, vol. 9, no. 4, pp. 533–537, Apr. 2020.
- [13] A. Zappone, M. Di Renzo, F. Shams, X. Qian, and M. Debbah, "Overhead-aware design of reconfigurable intelligent surfaces in smart radio environments," *arXiv preprint arXiv:2003.02538*, 2020.
- [14] D. Mishra and H. Johansson, "Channel estimation and low-complexity beamforming design for passive intelligent surface assisted MISO wireless energy transfer," in *Proc. Int. Conf. on Acoust., Speech, and Signal Process. (ICASSP)*, Brighton, UK, May 2019, pp. 4659–4663.
- [15] Z.-Q. He and X. Yuan, "Cascaded channel estimation for large intelligent metasurface assisted massive MIMO," *IEEE Wireless Commun. Lett.*, vol. 9, no. 2, pp. 210–214, Feb. 2020.
- [16] Z. Wang, L. Liu, and S. Cui, "Channel estimation for intelligent reflecting surface assisted multiuser communications: Framework, algorithms, and analysis," *IEEE Trans. Wireless Commun.*, vol. 19, no. 10, pp. 6607–6620, Apr. 2020.

$$\mathbb{E}_Y [p^\tau(\mathbf{Y})] = \int d(MK\mathbf{Q}_h)d(MN\mathbf{Q}_g)d(NK\mathbf{Q}_f)d(KT_p\mathbf{Q}_{x_p})d(KT_d\mathbf{Q}_{x_d})d(NT_p\mathbf{Q}_{c_p})d(NT_d\mathbf{Q}_{c_d}) \times p(\mathbf{Q}_h)p(\mathbf{Q}_g)p(\mathbf{Q}_f)p(\mathbf{Q}_{x_p}, \mathbf{Q}_{x_d})p(\mathbf{Q}_{c_p}, \mathbf{Q}_{c_d}) \mathbb{E}_{\mathbf{Z}_p, \mathbf{Z}_d} \left[\int d\mathbf{Y} \prod_{a=0}^{\tau} p(\mathbf{Y}|\mathbf{Z}^{(a)}) \right], \quad (61)$$

$$p\left(\left\{\left\{c_{nt}^{(a)}\right\}_{0 \leq a \leq \tau}; \mathbf{Q}_{x_p}, \mathbf{Q}_{x_d}, \mathbf{Q}_f\right\}\right) = \begin{cases} \delta(s_{nt} - 1)\mathcal{CN}\left(\left\{c_{nt}^{(a)}\right\}_{0 \leq a \leq \tau}; \mathbf{0}, [K\mathbf{Q}_f^{ab}\mathbf{Q}_{x_p}^{ab}]_{0 \leq a, b \leq \tau}\right) + \delta(s_{nt})\delta(c_{nt}), 1 \leq t \leq T_p, \\ \delta(s_{nt} - 1)\mathcal{CN}\left(\left\{c_{nt}^{(a)}\right\}_{0 \leq a \leq \tau}; \mathbf{0}, [K\mathbf{Q}_f^{ab}\mathbf{Q}_{x_d}^{ab}]_{0 \leq a, b \leq \tau}\right) + \delta(s_{nt})\delta(c_{nt}), T_p + 1 \leq t \leq T. \end{cases} \quad (62)$$

- [17] J. Chen, Y.-C. Liang, H. V. Cheng, and W. Yu. (Dec. 2019) Channel estimation for reconfigurable intelligent surface aided multi-user MIMO systems. [Online]. Available: <https://arxiv.org/abs/1912.03619>
- [18] H. Liu, X. Yuan, and Y.-J. A. Zhang, "Matrix-calibration-based cascaded channel estimation for reconfigurable intelligent surface assisted multi-user MIMO," *IEEE J. Sel. Areas Commun.*, vol. 38, no. 11, pp. 2621–2636, Nov. 2020.
- [19] T. L. Jensen and E. De Carvalho, "An optimal channel estimation scheme for intelligent reflecting surfaces based on a minimum variance unbiased estimator," in *ICASSP 2020-2020 IEEE International Conference on Acoustics, Speech and Signal Processing (ICASSP)*. IEEE, 2020, pp. 5000–5004.
- [20] L. Wei, C. Huang, G. C. Alexandropoulos, C. Yuen, Z. Zhang, M. Debbah *et al.*, "Channel estimation for ris-empowered multi-user MISO wireless communications," *arXiv preprint arXiv:2008.01459*, 2020.
- [21] A. M. Elbir, A. Papazafeiropoulos, P. Kourtessis, and S. Chatzinotas, "Deep channel learning for large intelligent surfaces aided mm-wave massive MIMO systems," to appear at *IEEE Wireless Commun. Lett.*, DOI: 10.1109/LWC.2020.2993699.
- [22] S. Liu, Z. Gao, J. Zhang, M. Di Renzo, and M.-S. Alouini, "Deep denoising neural network assisted compressive channel estimation for mmwave intelligent reflecting surfaces," *arXiv preprint arXiv:2006.02201*, 2020.
- [23] D. L. Donoho, A. Maleki, and A. Montanari, "Message-passing algorithms for compressed sensing," *Proc. Natl. Acad. Sci.*, vol. 106, no. 45, pp. 18 914–18 919, 2009.
- [24] S. Rangan, "Generalized approximate message passing for estimation with random linear mixing," in *Proc. IEEE Int. Symp. Inf. Theory*, Aug. 2011, pp. 2168–2172.
- [25] J. T. Parker, P. Schniter, and V. Cevher, "Bilinear generalized approximate message passing—Part I: Derivation," *IEEE Trans. Signal Process.*, vol. 62, no. 22, pp. 5839–5853, Nov. 2014.
- [26] H. Nishimori, *Statistical Physics of Spin Glasses and Information Processing: An Introduction*. Oxford, U.K.: Oxford Univ. Press, 2001, no. 111 in International Series of Monographs on Physics.
- [27] Y. Kabashima, F. Krzakala, M. Mézard, A. Sakata, and L. Zdeborová, "Phase transitions and sample complexity in Bayes-optimal matrix factorization," *IEEE Trans. Inf. Theory*, vol. 62, no. 7, pp. 4228–4265, Jul. 2016.
- [28] B. Zheng and R. Zhang, "Intelligent reflecting surface-enhanced ofdm: Channel estimation and reflection optimization," *IEEE Wireless Communications Letters*, vol. 9, no. 4, pp. 518–522, 2019.
- [29] C.-K. Wen, C.-J. Wang, S. Jin, K.-K. Wong, and P. Ting, "Bayes-optimal joint channel-and-data estimation for massive MIMO with low-precision ADCs," *IEEE Trans. Signal Process.*, vol. 64, no. 10, pp. 2541–2556, May 2016.
- [30] R. Prasad, C. R. Murthy, and B. D. Rao, "Joint channel estimation and data detection in MIMO-OFDM systems: A sparse bayesian learning approach," *IEEE Trans. Signal Process.*, vol. 63, no. 20, pp. 5369–5382, 2015.
- [31] E. Nayebi and B. D. Rao, "Semi-blind channel estimation for multiuser massive MIMO systems," *IEEE Trans. Signal Process.*, vol. 66, no. 2, pp. 540–553, 2017.
- [32] S. Guo, S. Lv, H. Zhang, J. Ye, and P. Zhang. (May 2020) Reflecting modulation. [Online]. Available: <https://arxiv.org/abs/1912.08428>
- [33] W. Yan, X. Yuan, Z.-Q. He, and X. Kuai, "Passive beamforming and information transfer design for large intelligent surface aided multiuser MIMO systems," *IEEE J. Sel. Areas Commun.*, vol. 38, no. 8, pp. 1793–1808, Jun. 2020.
- [34] S. Wu, L. Kuang, Z. Ni, D. Huang, Q. Guo, and J. Lu, "Message-passing receiver for joint channel estimation and decoding in 3D massive MIMO-OFDM systems," *IEEE Trans. Wireless Commun.*, vol. 15, no. 12, pp. 8122–8138, 2016.
- [35] J. Zhang, X. Yuan, and Y.-J. A. Zhang, "Blind signal detection in massive MIMO: Exploiting the channel sparsity," *IEEE Trans. Commun.*, vol. 66, no. 2, pp. 700–712, Feb. 2018.
- [36] J. G. Proakis, *Digital Communications*. McGraw Hill, 4th ed., 1995.
- [37] S. L. Loyka, "Channel capacity of mimo architecture using the exponential correlation matrix," *IEEE Commun. Lett.*, vol. 5, no. 9, pp. 369–371, Sep. 2001.
- [38] T. Tanaka, "A statistical-mechanics approach to large-system analysis of cdma multiuser detectors," *IEEE Trans. Inf. Theory*, vol. 48, no. 11, pp. 2888–2910, 2002.
- [39] H. Touchette, "A basic introduction to large deviations: Theory, applications, simulations," *arXiv preprint arXiv:1106.4146*, 2011.

$$\mathcal{I}_h = \mathbb{E}_{h'} \left\{ \int dy_h e^{-|y_h - \sqrt{\tilde{m}_h} h'|^2} \left(\mathbb{E}_h \left[e^{-\tilde{m}_h |h|^2 + 2\sqrt{\tilde{m}_h} \text{Re}(y_h^* h)} \right] \right)^\tau \right\} - (\tau + 1) q_h \tilde{q}_h - (\tau^2 + \tau) \tilde{m}_h m_h \quad (84)$$

$$\begin{aligned} \mathcal{F} = & \frac{2M}{K^2} \sum_{o \in \{p, d\}} T_o \ln \left(\mathbb{E}_{v, u'} \left[\int dy \mathcal{N}(y; \sqrt{q_{z_o} - m_{z_o}} u' + \sqrt{m_{z_o}} v; \sigma^2) \ln \mathbb{E}_u \left\{ \mathcal{N}(y; \sqrt{q_{z_o} - m_{z_o}} u + \sqrt{m_{z_o}} v; \sigma^2) \right\} \right] \right) \\ & + \frac{M}{K} \left(\mathbb{E}_{h'} \left\{ \int dy_h e^{-|y_h - \sqrt{\tilde{m}_h} h'|^2} \ln \mathbb{E}_h \left[e^{-\tilde{m}_h |h|^2 + 2\sqrt{\tilde{m}_h} \text{Re}(y_h^* h)} \right] \right\} - \tilde{m}_h m_h \right) \\ & + \frac{MN}{K^2} \left(\mathbb{E}_{g'} \left\{ \int dy_g e^{-|y_g - \sqrt{\tilde{m}_g} g'|^2} \ln \mathbb{E}_g \left[e^{-\tilde{m}_g |g|^2 + 2\sqrt{\tilde{m}_g} \text{Re}(y_g^* g)} \right] \right\} - \tilde{m}_g m_g \right) \\ & + \frac{1}{K} \sum_{o \in \{p, d\}} T_o \left(\mathbb{E}_{x'_o} \left\{ \int dy_{x_o} e^{-|y_{x_o} - \sqrt{\tilde{m}_{x_o}} x'_o|^2} \ln \mathbb{E}_{x_o} \left[e^{-\tilde{m}_{x_o} |x_o|^2 + 2\sqrt{\tilde{m}_{x_o}} \text{Re}(y_{x_o}^* x_o)} \right] \right\} - \tilde{m}_{x_o} m_{x_o} \right) \\ & + \frac{N}{K^2} \sum_{o \in \{p, d\}} T_o \left(\mathbb{E}_{c'_o} \left\{ \int dy_{c_o} e^{-|y_{c_o} - \sqrt{\tilde{m}_{c_o}} c'_o|^2} \ln \mathbb{E}_{c_o} \left\{ e^{-\tilde{m}_{c_o} |c_o|^2 + 2\sqrt{\tilde{m}_{c_o}} \text{Re}(y_{c_o}^* c_o)} \right\} \right\} - \tilde{m}_{c_o} m_{c_o} \right) \quad (85) \end{aligned}$$